

Entrainment and motion of coarse particles in a shallow water stream down a steep slope

By C. ANCEY¹, A.C. DAVISON², T. BÖHM³, M. JODEAU⁴,
AND P. FREY³

¹School of Architecture, Civil and Environmental Engineering,
École Polytechnique Fédérale de Lausanne, 1015 Lausanne, Switzerland

²Institute of Mathematics,
École Polytechnique Fédérale de Lausanne, 1015 Lausanne, Switzerland

³Cemagref, Domaine Universitaire BP 76, 38402 Saint-Martin-d'Hères Cedex, France

⁴Cemagref, 3 bis quai Chauveau, 69336 Lyon, France

(Report date: October 2006)

In this paper we investigate the entrainment, deposition, and motion of coarse spherical particles within a turbulent shallow water stream down a steep slope. This problem is an idealization of bed-load transport in gravel-bed rivers. Earlier investigations have described this kind of sediment transport using empirical correlations or concepts borrowed from continuum mechanics. The intermittent character of particle transport at low water discharges led us to consider it as a random process. As suggested more than fifty years ago, sediment transport in this regime results from the imbalance between entrainment and deposition of particles rather than momentum balance between water and particles. We develop a birth-death immigration-emigration Markov process to describe the particle exchanges between the bed and the water stream. A key feature of the model is the existence of rather long autocorrelation times and wide, frequent fluctuations in the solid discharge, a troublesome phenomenon never previously explained despite its ubiquity in both nature and laboratory experiments. We then present experimental data obtained using a nearly two-dimensional channel and glass beads as a substitute for sediment. Entrainment, trajectories, and deposition were monitored using a high-speed digital camera, which filmed the channel from the side. The theoretical model was tested against these data. The probability distributions of the solid discharge and deposition frequency were properly described by the model. Experiments confirmed the existence of wide and frequent fluctuations of the solid discharge. They also revealed the existence of long autocorrelation time, but theory overestimates the autocorrelation times by a factor of around three. A striking feature is that particle velocity was weakly dependent on the fluid velocity contrary to the predictions of the theoretical model, which performs well when a single particle is moving. The consequence is that for our experiments, the dependence of the solid discharge on the fluid velocity is entirely controlled by the number of moving particles rather than by their velocity. We also noted significant changes in the behaviour of particle transport when the bed slope or the water discharge was increased. The more vigorous the stream was, the more continuous the solid discharge became. Moreover, while 90% of the energy supplied by gravity to the stream is dissipated by turbulence for slopes lower than 10%, particles dissipate more and more energy when the bed slope is increased, but surprisingly enough, the dissipation rate is nearly independent of fluid velocity.

1. Introduction

A longstanding problem in the study of bed load transport in gravel-bed rivers is related to the physical mechanisms governing bed resistance and particle motion. Although experimental investigations have been conducted over the last three decades, there remains a wide gap between field measurements and the predictions of theoretical models, despite their capacity to describe bed load transport for laboratory experiments correctly. For instance, the sediment flow rates measured in gravel-bed rivers differ within one to two orders of magnitude from the solid discharges predicted by bed-load transport equations (Gomez & Church 1989; Wilcock 2001; Martin 2003; Barry *et al.* 2004), although these equations have been established from flume experiments using regression techniques and are believed to provide a proper evaluation of sediment transport in a well-controlled laboratory environment.

At first sight, this appears paradoxical, because experiments usually show simple behaviour, e.g., a linear or pseudo-linear dependence of the solid discharge on the water discharge (Bagnold 1986). Over the last century this has led to attempts to develop an analytical model for computing the transport rate of sediment in rivers. Of the numerous mechanistic descriptions of bed load transport, two main approaches have emerged: Bagnold's and Einstein's formulations (Graf 1984; Raudkivi 1990; Seminara *et al.* 2002).

In Bagnold's mind, the solid discharge equation can be derived by considering the balance between the energy supplied by gravity and that expended by turbulence and sediment transport (Bagnold 1966, 1973). In Bagnold's model and subsequent variants (Bridge & Dominic 1984; Wiberg & Smith 1989; van Rijn 1985; Niño & García 1998), bed load transport is essentially a two-phase flow, the dynamics of which is controlled by the momentum transfers between the water and solid phases. When compared with laboratory experimental data or field measurements, Bagnold's scaling correctly describes the sediment transport for steady uniform or gently varying flows at sufficiently high solid discharges (Julien 1994). However, there are several indications that Bagnold's formulation may be flawed or crude. First, for this scaling to match experimental observations, the bulk particle friction coefficient introduced by Bagnold must be fitted to nonphysical values (Fernandez Luque & van Beek 1976; Niño *et al.* 1994). Second, for flow conditions that depart from steady uniform flow conditions, Bagnold's model yields poor results, notably for flows over arbitrarily sloping beds (Seminara *et al.* 2002) or at low levels of solid discharge (Fernandez Luque & van Beek 1976; Nelson *et al.* 1995). Third, if bed-forms (dune or antidune depending on the value of the Froude number) are interpreted as resulting from a loss of linear stability in the coupled fluid-solid system, Bagnold's model fails to capture the necessary physics, since the corresponding equations of motion show no instability (Balmforth & Provenzale 2001).

In Einstein's view, sediment transport does not result from an equilibrium in the momentum transfers between solid and liquid phases, but rather from the difference between the entrainment and deposition rates, E and D , respectively, which are a function of the flow conditions and bed geometry (Einstein 1950; Ettema & Mutel 2004). This amounts to writing that on a small interval Δx , the solid discharge variation is $\delta q_s = (E - D)\Delta x$, and so the solid discharge at bed equilibrium is the implicit solution to the equation $E = D$. Einstein's stochastic approach poses several problems that have as yet few possible solutions. For instance, as particles move sporadically and in different groups, the solid flow rate comprises a series of pulses and is highly fluctuating, making it difficult to define and measure it properly, even under steady flow conditions (Bunte & Abt 2005). Another problem is the proper definition of the characteristic time of entrainment and deposition rates, controversy about which has led to several attempts

to refine Einstein's original formulation (Laursen 1958, 1999; Paintal 1971; Lopez & Garcia 2001; Kleinhans & van Rijn 2002; Cheng 2004; Cheng *et al.* 2004; Charru *et al.* 2004). Other aspects, such as the abnormal diffusion of bed particles or wide fluctuations in the solid discharge, seriously conflict with the predictions of Einstein-like theories and question their statistical basis (Nikora *et al.* 2001, 2002; Ancey *et al.* 2006)—both field and laboratory experiments have revealed that cases in which the instantaneous solid discharge is three to four times higher than its mean value are frequent (Kuhnle & Southard 1988; Lisle 1989; Böhm *et al.* 2004), suggesting that the probability density functions of the transport-rate records have a thick tail and thus depart from the expected Gaussian behaviour. This can be seen as the hallmark of collective motions (Sornette 2000); if so, it also undermines any mean-field approximation under which cooperation between particles is unaccounted for.

Both approaches provide solid discharge equations that are in fairly good agreement with flume experiments in the laboratory and, to some degree, with field measurements in rivers, but both rely on empirical parameters and thus require the use of fitting procedures. Indeed, a full analytical approach is almost intractable owing to the many processes involved: complex interplay between the particles and the carrying fluid; particle exchanges between the bed and the flow; turbulence effects (bed friction, advection of turbulent structures); and so forth. In this and in many other problems in the environmental sciences, it is difficult to judge the reliability of a model of which some, if not all, parameters have to be tuned (Iverson 2003). The measure of success of a theory is seriously biased by the systematic and unavoidable recourse to parameter fitting. Rather than seeking immediate applicability, progress requires an enhanced understanding of physical processes and the testing of models by assessing the extent of the range over which the discrepancies with measurements are minor. Moreover, if one focuses on solving all the specific problems of turbulent flow in particle systems, one may lose sight of the original objective, of finding a simple but general analytical framework for dealing with sediment-transport issues in practical situations.

The present paper is a step towards such a framework, made by thoroughly examining various physical processes involved in sediment transport, while keeping a reasonable level of complexity in our description. A key factor was to be able to access the details of the flows and measure as much parameters as possible. Also, to avoid complications associated with many laboratory experiments when working with natural sediment, we devised a simple system in which the boundary and initial conditions can be entirely controlled and imposed. We built a narrow channel, in which sediment was replaced by coarse spherical glass beads. As our aim was not to provide a comprehensive picture of sediment transport, we focused on steep slopes and coarse particles, for which transport of particles is referred to as bedload transport—particles are not in suspension, but roll or jump along the bed. The resulting flow conditions are typical of those encountered in gravel-bed rivers in piedmont and mountain regions.

Section 2 outlines our theoretical framework. We wish to compute the solid discharge, which can be defined as the product of the number of moving particles and the mean particle velocity. In any theory of sediment transport, the crux of the issue lies in the proper evaluation of the number of particles entrained and maintained in motion by the water stream. In Bagnold's approach, sediment transport results from an equilibrium in the momentum transfer between solid and liquid phases. The number of moving particles is then found to be the ratio between the available energy and that expended during the motion of one particle due to momentum transfers between the solid and liquid phases. The mean-field treatment applied by Bagnold conflicts with a noticeable feature of sediment transport: its intermittent nature at low flow rates. Both laboratory and field

measurements reveal that particle movement occurs for a period of time followed by a period in which no motion occurs (Grass 1970; Drake *et al.* 1988; Niño & García 1998). At low flow rates, intermittent motion occurs when the near-bed downstream velocity is sufficiently high to destabilize stationary particles and set them in motion. This situation corresponds to instances in which the instantaneous near-bed velocity outweighs its mean value as a result of near-bed turbulence and does not correlate well with the mean flow conditions far from the bed (Nelson *et al.* 1995, 2001; Schmeeckle & Nelson 2003). In Einstein’s theory, sediment transport results from the imbalance between entrainment and deposition. Intermittency in particle motion is usually taken into account by treating it as a two-state Markov process (Lisle *et al.* 1998; Papanicolaou *et al.* 2002; Ancey *et al.* 2006). A severe shortcoming with existing models of whatever sophistication is that they give unrealistic statistical distributions of the solid discharge fluctuations; for instance, they predict that the solid discharge gently fluctuates around its mean value for equilibrium flow conditions, whereas experiments reveal the existence of wide and frequent fluctuations (Ancey *et al.* 2006). Here, we develop a generalized birth-death Markov process to describe the time variation in the number of moving particles. This rather simple stochastic model is able to overcome the current limitations of Einstein-like models and to predict a number of interesting features, such as the autocorrelation time of the solid discharge.

In § 3 we describe our experimental facility. We run experiments in an inclined, tight flume with a continuous particle supply and steady flow rate. This nearly two-dimensional flume is assumed to be the simplest representation of sediment transport on the laboratory scale and presents overwhelming advantages: the boundary conditions can be controlled and most of the flow variables can be measured by image processing. Section 4 is devoted to experimental results and comparison with our theoretical model. Since a quantitative comparison between theory and experiment is biased by any parameter fitting, we test theory by analyzing the probabilistic features of the model. In § 5 we summarize our more interesting findings and look ahead a little.

2. Theoretical framework

2.1. Objective and notation

We consider a two-dimensional, steady water stream flowing down a bed, the mean slope of which is denoted by θ . The bed is made up of mobile spherical particles of equal radius a and density ρ_p . The water flow rate per unit width q_w is prescribed at the channel entrance, and the flume is supplied with particles identical to those making up the bed. Figure 1 shows the flow configuration.

A few solid particles are entrained by the water stream: they can roll/slide along the bed or they can leap and stay in saltation in the water stream for short time periods. We refer to the former motion as the *rolling regime* and to the latter as the *saltating regime*. As we are especially interested in weakly intense bed-load transport, we stress flows with a fairly low fluid velocity; in this case the trajectory of a single particle exhibits a succession of rests and moves in a rolling or saltating regime, which making it difficult to discriminate the motion regime accurately. Here we no longer discriminate between rolling and saltation, except when stated explicitly, and treat both these motions as a single species which we call the moving particles.

In a typical bed-load transport problem, knowing the control parameters of this flow configuration (q_w , θ , a , ρ_p), we wish to determine the flow properties: the flow depth h ; the solid discharge q_s , that is, the number of particles per unit time conveyed by the flow,

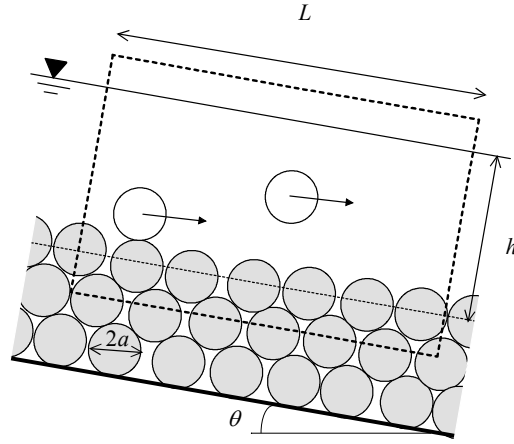


FIGURE 1. Sketch defining the flow configuration.

measured in m^3/s ; and the mean flow $\bar{u}_f = q_w/h$. Hence we consider a control volume \mathcal{V} within which we follow the particles and the motion of the fluid; we pose $V = \mathcal{S} \times L$, where the length is denoted by L , the volume by V , and the cross-section by $\mathcal{S} = hW$, where W represents the flume width.

In this section we restrict our attention to sediment transport at equilibrium, i.e., on average, flow is steady and there is neither deposition nor erosion along the bed. In the next subsection we show that the solid discharge can be computed as $q_s \propto N\bar{u}_p$, where N denotes the number of particles within the control volume \mathcal{V} and \bar{u}_p is the mean particle velocity. In § 2.2 we develop a stochastic model for the number of particles in \mathcal{V} , while § 2.5 is devoted to particle velocity. In § 2.2 we derive the so-called master equation, a partial differential equation governing the time variations in $P(n;t)$, with $P(n;t)$ the probability of finding $N = n$ moving particles in the control volume at time t . General and stationary solutions to the master equation are derived in § 2.3 and § 2.4, respectively.

2.2. Birth-death emigration-immigration process

The solid discharge can be defined as the flux of particles through a flow cross-section \mathcal{S} : $q_s = \int_{\mathcal{S}} \mathbf{u}_p \cdot \mathbf{k} d\mathcal{S}$, where \mathbf{k} is the unit normal to \mathcal{S} . This definition, suitable for continuous fields, is not well suited to discrete elements, for which it is more convenient to introduce the flow rate in terms of the probability $P[\mathbf{u}_p | \mathbf{x}, t]$ that a particle crosses the control surface \mathcal{S} at position \mathbf{x} and time t with velocity \mathbf{u}_p ,

$$q_s = \int_{\mathcal{S}} \int_{\mathbb{R}^2} P[\mathbf{u}_p | \mathbf{x}, t] \mathbf{u}_p \cdot \mathbf{k} |d\mathbf{x}| d\mathbf{u}_p. \quad (2.1)$$

Under steady conditions we have $\partial P/\partial t = 0$ and so this definition reduces to

$$q_s = \lim_{V \rightarrow \infty} \frac{1}{V} \sum_{i=1}^N u_i v_p \mathcal{S} = \lim_{L \rightarrow \infty} \frac{v_p}{L} \sum_{i=1}^N u_i, \quad (2.2)$$

where the ensemble average has been replaced by a volume average and v_p is the particle volume. Integration has been performed over the control volume \mathcal{V} . We have also used $u_i = \mathbf{u}_p \cdot \mathbf{k}$ to denote the streamwise velocity component of particle i , and N to denote the number of moving particles within the control volume. Below we shall define the flow

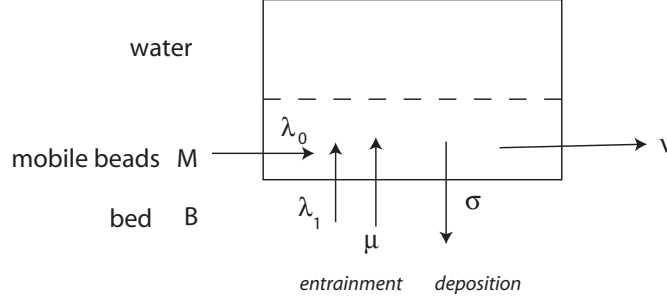


FIGURE 2. The number of moving beads observed within the window varies with time depending on the number of particles entering/leaving the window or being entrained/deposited from/on the stationary bed.

rate $\dot{n} = q_s/v_p$ as

$$\dot{n} = \frac{1}{L} \sum_{i=1}^N u_i. \quad (2.3)$$

In order to compute the discharge equation, we need to establish the number N of particles in motion and their velocities, which depend on the control parameters (q_w , θ , a , ϱ_p). We assume that the number of stationary beads within the bed is infinite.

We now consider the total number $N(t)$ of particles in motion within the control volume \mathcal{V} at time t . Figure 2 sketches the particle exchanges within the control volume. We describe sediment transport using an immigration-emigration birth-death model, which is a particular generalized Markov birth process (Cox & Miller 1965), using the following exchanges:

- A moving bead enters the window at rate $\lambda_0 > 0$ by rolling/saltation from the left (immigration). The probability that a particle arriving into the window in the time interval t and $t + \Delta t$ is independent of t and N and we can write

$$P(n \rightarrow n+1; \Delta t) = \lambda_0 \Delta t + o(\Delta t).$$

- Moving beads leave the window independently at rate $\nu > 0$ (emigration). The transition probability is

$$P(n \rightarrow n-1; \Delta t) = n\nu \Delta t + o(\Delta t).$$

- Two processes enable entrainment of particles from the bed (birth): an individual particle can be dislodged from the bed by the water stream at rate $\lambda_1 > 0$; or a moving bead can hit a stationary one and set it moving. This occurs at rate μ for any moving bead within the observation window. In the former case, the related transition probability is

$$P(n \rightarrow n+1; \Delta t) = \lambda_1 \Delta t + o(\Delta t),$$

while in the latter case, it can be expressed as

$$P(n \rightarrow n+1; \Delta t) = \mu n \Delta t + o(\Delta t).$$

- A moving bead can settle (i.e., come to rest) within the window, independently at rate σ for each moving bead (death). The transition probability is thus

$$P(n \rightarrow n-1; \Delta t) = n\sigma \Delta t + o(\Delta t).$$

With these assumptions and using the usual arguments for setting up the forward

equations of a Markov process with discrete states in continuous time (Cox & Miller 1965; Gardiner 1983), we obtain a set of equations

$$P(n; t + \Delta t) = \alpha(n+1)\Delta t P(n+1; t) + P(n-1; t)(\lambda + (n-1)\mu)\Delta t + P(n; t)(1 - \Delta t(\lambda + n\alpha + n\mu)) + o(\Delta t),$$

for $n = 1, 2, \dots$, and

$$P(0; t + \Delta t) = \alpha P(1; t)\Delta t + P(0; t)(1 - \lambda\Delta t) + o(\Delta t),$$

for $n = 0$, with the short-hand notation $\alpha = \sigma + \nu$ and $\lambda = \lambda_1 + \lambda_0$. The time increment Δt is assumed to be sufficiently small that two events cannot occur in $(t, t + \Delta t)$. On rearranging the terms and letting $\Delta t \rightarrow 0$, we arrive at the following master equation describing the time variation in $P(n; t)$:

$$\frac{\partial}{\partial t} P(n; t) = (n+1)\alpha P(n+1; t) + (\lambda + (n-1)\mu) P(n-1; t) - (\lambda + n(\alpha + \mu)) P(n; t), \quad (2.4)$$

$$\frac{\partial P}{\partial t}(0, t) = \alpha P(1; t) - \lambda P(0; t). \quad (2.5)$$

The initial condition specifies that at time $t = 0$, there are $N = N_0$ particles within the control volume, so we set

$$P(n; 0) = \delta(n - N_0), \quad (2.6)$$

where δ is the Kronecker delta function.

We now discuss the main assumptions underlying equation (2.4). Both entrainment processes deserve further attention since they are the cornerstone of this theoretical description. Another key point is related to the physical origin of the mathematical formulation, its limitations, and the nature of the parameters λ_0 , λ_1 , μ , ν , and σ .

The main originality of the model lies in the treatment of particle entrainment. In Einstein-like theories, particles are entrained because the drag/lift force exerted by the water stream sometimes exceeds the resisting force (weight and bed friction) of a stationary particle (see below) and there is no collective entrainment ($\mu = 0$). This results in a purely Poissonian representation of particle entrainment (Lisle *et al.* 1998; Papanicolaou *et al.* 2002; Ancey *et al.* 2006). This kind of entrainment reflects the erosive action of water and thus is independent of the number of particles previously entrained. It also implies that the total number of moving particles varies little with time, i.e., the variance of N should be lower than its mean, in conflict with experimental and field observations (Ancey *et al.* 2006). Here we include an additional entrainment process, which depends on the number of moving particles and reflects the destabilization of bed particles and their entrainment due to collisions with moving particles, which was clearly identified in experiments and field surveys (Drake *et al.* 1988; Böhm *et al.* 2004). The effect would be close to the *splash* function used for modelling sand drift (sand transport induced by wind), although the physical processes are quite different. As shown later, this kind of entrainment allows the probability distribution function of N to accommodate the wide fluctuations of N seen in experiments. Although we sought alternative models for collective entrainment, for instance by relating the probability of entrainment and local particle arrangement, we failed to find a typical scenario supporting this idea. After many trials, this assumption on collective entrainment was the simplest and most efficient we could find.

Our statistical approach is likely to perform for a finite range of water flow rates. Indeed, the flow rate must be sufficiently high for the probability of entrainment to be appreciable, but not so high that entrainment occurs intermittently. This idea and its implications can be more easily understood using Figure 3, which represents the time

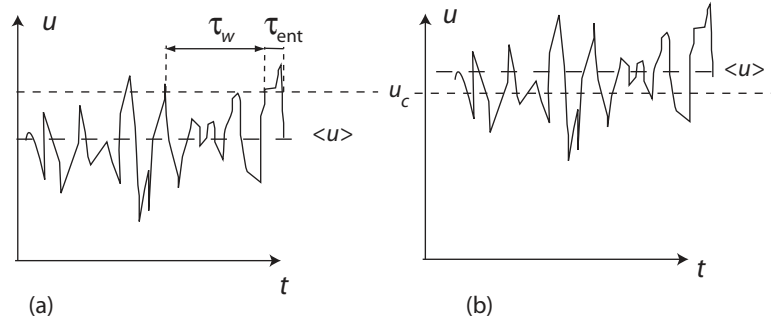


FIGURE 3. Fluctuations of the instantaneous velocity u around the mean value $\langle u \rangle$. (a) Mean fluid velocity below the critical threshold u_c . (b) Mean fluid velocity in excess of the critical threshold u_c . In both cases, particle entrainment occurs sporadically.

variations in the instantaneous fluid velocity u seen by a bed particle under steady flow conditions. The mean fluid velocity is denoted by $\langle u \rangle(y)$, where y is the height from a reference level and the brackets stand for time-averaged values. The force exerting on the particle by the fluid is usually split into three contributions: hydrostatic pressure, drag, and lift. In the current models of entrainment on steep slopes, a particle is set in motion whenever the combined action of gravity and fluid forces exceeds the particle weight and the frictional force (Armanini & Gregoretti 2005); since in these models, the mean lift and drag forces are directly linked to the mean fluid velocity $\langle u \rangle(y)$, loss of stability and incipient motion occur whenever the instantaneous fluid velocity exceeds a critical threshold u_c , which depends on bed slope, particle arrangement, and so forth (Kirchner *et al.* 1990; Armanini & Gregoretti 2005). The probability of entrainment is thus the exceedance probability $P(u > u_c)$ (Einstein 1950; Papanicolaou *et al.* 2002).

To determine how frequently these events occur, we require the characteristic time between two events. We refer to τ_w as the waiting time between events, while the mean duration of an entrainment event (i.e., during which $P(u > u_c)$) is denoted by τ_{ent} . [see Figure 3(a)]. The exceedance probability $P_c = P(u > u_c)$ gives the time ratio $\tau_e/(\tau_w + \tau_e)$. We introduce the Taylor macro scales of length and time, L_x and time $\tau_{turb.}$, which represent the correlation length and time of large turbulent structures, respectively. For open channel flows down rough surfaces, semi-empirical models give estimates of the large-eddy length scale in the form $L_x = Ah\sqrt{y/h}$, where A is a constant close to unity (Nezu & Nakagawa 1993); for steady flow conditions, the autocorrelation time macro scale is then $\tau_{turb.} = L_x/\langle u \rangle$. Assuming that the autocorrelation time function can be approximated by an exponential function, and using $1/\tau_{turb.} = 1/\tau_w + 1/\tau_{ent.}$, we deduce that the waiting time is

$$\tau_w = \frac{1 - P_c^2}{P_c} \frac{L_x}{\langle u \rangle} : \quad (2.7)$$

thus the entrainment rate $\lambda_1 \propto \tau_w^{-1}$ varies nonlinearly with the fluid velocity $\langle u \rangle$. Equation (2.7) also shows that for nearly constant probabilities P_c (i.e., when the mean fluid velocity varies within less than one order of magnitude), λ_1 scales linearly with the fluid velocity, while keeping the fluid velocity constant and increasing fluid turbulence (thus letting P_c to 1) increases entrainment rate substantially. This behaviour is consistent with experimental observations at intermediate bottom shear stress (Sumer *et al.* 2003; Cheng 2004).

This statistical description is likely to hold at intermediate bottom shear stress, i.e., for $\langle u \rangle < u_c$ [see Figure 3(a)] or $\langle u \rangle > u_c$ [see Figure 3(b)] provided that $|\langle u \rangle - u_c| < u'$,

where u' denotes the root mean square velocity in the streamwise direction. Indeed, at very low shear stress, i.e., when $\langle u \rangle$ is far below the critical threshold, entrainment may occur on rare occasions when turbulent eddies that are on the same scale as the particle produce imbalanced pressure fields around the particle, leading to a high lift event; such events are strongly dependent on the details of the flow around of the particle and particle arrangement of the bed, which cannot be conveniently related to the average conditions (Nelson *et al.* 2001). Extreme value theory suggests that the number of instances in which a particle is lifted up from the bed will follow a Poisson distribution (Coles 2001), but with a rate λ_1 independent of the mean velocity. Conversely, at high bottom shear stress (i.e., for $\langle u \rangle \gg u_c$), any bed particle exposed to the stream is instantaneously set in motion. In that case, bed load transport takes the form of a sheet flow separating the bed from the water flow (Jenkins & Hanes 1998). This continuous process cannot readily be described within our stochastic framework.

2.3. General solution

We obtain the general solution to the forward master equations (2.4)–(2.5) subject to the initial condition (2.6). This solution can be found by introducing the probability generating function (Gardiner 1983)

$$G(z, t) = \sum_{n=0}^{\infty} z^n P(n; t),$$

which makes it possible to transform the master equations into a single partial differential equation. Multiplying equations (2.4)–(2.5) by z^n and summing the terms, we obtain

$$\frac{\partial}{\partial t} G(z, t) = \lambda(z-1)G(z, t) + (\sigma + \mu z^2 + \nu - (\mu + \sigma + \nu)z) \frac{\partial}{\partial z} G(z, t). \quad (2.8)$$

This first-order linear equation can be solved by seeking the first integrals of the associated characteristic equations (Garabedian 1964)

$$\frac{dt}{1} = \frac{dz}{(\alpha - \mu z)(z-1)} = \frac{dG}{\lambda(z-1)G}. \quad (2.9)$$

These first integrals are easily seen to be

$$t = \frac{1}{\alpha - \mu} \ln \frac{|z-1|}{|\alpha - z\mu|} + c_1 \quad \text{and} \quad G = c_2 |\alpha - z\mu|^{-\lambda/\mu},$$

where c_1 and c_2 are two constants of integration. The general solution to equation (2.8) is thus a combination of the two independent first integrals

$$G(z, t) = (\alpha - z\mu)^{-\lambda/\mu} f \left(e^{-t(\alpha-\mu)} \frac{1-z}{\alpha - z\mu} \right), \quad (2.10)$$

since $z < 1$ and provided that $\alpha > \mu$ (see § 2.4) so that a stationary solution exists. The function f in equation (2.10) is determined using the initial condition. At time $t = 0$, if there are $n = N_0$ beads within the control volume, setting $t = 0$ in (2.10) yields

$$G(z, 0) = z^n = (\alpha - z\mu)^{-\lambda/\mu} f \left(\frac{1-z}{\alpha - z\mu} \right),$$

from which we obtain

$$f(x | N_0 = n) = \left(\frac{1 - \alpha x}{1 - \mu x} \right)^n \left(\frac{\alpha - \mu}{1 - \mu x} \right)^{\lambda/\mu}.$$

Thus the complete form of G , given that the initial state is known, is

$$G(z, t | N_0 = n) = \left(\frac{\alpha - \mu}{(K\mu - \mu)z + \alpha - K\mu} \right)^{n+\lambda/\mu} \left(\frac{(K\alpha - \mu)z + \alpha(1-K)}{\alpha - \mu} \right)^n, \quad (2.11)$$

where $K = e^{-t(\alpha-\mu)}$; we shall see in § 2.4 that the function K corresponds to the autocorrelation function for flows at equilibrium. Equation (2.11) can be interpreted as the convolution product[†] of independent binomial and negative variables S and T : $S \sim \text{Bin}(n, p_0)$ and $T \sim \text{NegBin}(n + \lambda/\mu, p_1)$, with $p_0 = (K\alpha - \mu)/(\alpha - \mu) < 1$ and $p_1 = (\alpha - \mu)/(\alpha - K\mu) < 1$. With this decomposition in mind, we could interpret G as the probability generating function of the random variable $N = S + T$. This decomposition makes sense only at short times: at long times, $K \rightarrow 0$ and so p_0 becomes negative. At short times, this decomposition would mean that the random variations in N result from two independent processes. To see the relative strength of each contribution over time, let us compute the ratio of the mean of S to that of T ,

$$\frac{n}{\alpha - \mu} \frac{(K\alpha - \mu)^2}{(1-K)(\alpha n + \lambda)} \propto \frac{n}{\alpha n + \lambda} \frac{\alpha - \mu}{1-K} \text{ for } t \rightarrow 0;$$

at short times ($t \rightarrow 0$, $K \rightarrow 1$), the contribution of S prevails over that of T , but the latter becomes increasingly important as time increases.

The generating function gives the transition probability $\text{Prob}(N(t) = m | N(0) = n)$, which is the coefficient of z^m in the power series expansion of $G(z, t | N_0 = n)$. This may be used to estimate the parameters α , λ , and μ when the system is out of equilibrium, as is often the case for laboratory and field measurements.

As expected, $G(1, t) = 1$ and $G(z, 0) = z^n$. When $\mu = 0$, G is the probability generating function of the binomial distribution $\text{Bin}(n, K)$, and we retrieve the behaviour expected under Einstein's theory (Ancey *et al.* 2006): the sporadic motion of each particle is described as a Bernoulli process, and as the sum of N Bernoulli processes is a binomial process, N behaves like a binomial variable.

2.4. Steady-state solution

For steady flow conditions, the number of particles within the observation window forms a stationary random process, which can be completely described by its probability distribution and its autocorrelation function. First, we find the stationary probability distribution $P_s(n) = \text{Prob}(N = n)$ to which $P(n; t)$ tends when the average flow conditions are steady.

For steady-state conditions, G is independent of t and we express it as $G_s(z)$. Equation (2.8) reduces to an ordinary differential equation

$$\frac{1}{G_s} \frac{dG_s}{dz} = \frac{\lambda}{\alpha - \mu z},$$

with the boundary condition $G_s(1) = 1$.

For $\mu > 0$, integrating this equation leads to

$$G_s(z) = \left(\frac{\alpha - \mu}{\alpha - \mu z} \right)^{\lambda/\mu},$$

[†] Recall that the generating function is directly linked to the characteristic function $\phi(s) = \sum_k e^{isk} P(k)$ by posing $G(z) = \phi(-i \ln z)$ (Gardiner 1983). The characteristic function of the sum of independent random variables is given by the product of the characteristic functions of these variables.

the probability generating function of the negative binomial distribution

$$P_s(n) = \text{NegBin}(n; r, p) = \frac{\Gamma(r+n)}{\Gamma(r)n!} p^r (1-p)^n, n = 0, 1, \dots, \quad (2.12)$$

with $r = \lambda/\mu$ and $p = 1 - \mu/\alpha$, and where Γ denotes the gamma function (Davison 2003). The mean is $\lambda/(\alpha - \mu)$ and the variance is

$$\text{Var}(N) = \frac{\lambda\alpha}{(\alpha - \mu)^2}. \quad (2.13)$$

For $\mu = 0$, we obtain $G_s(z) = e^{-\lambda(z-1)/\alpha}$, corresponding to the Poisson distribution of rate $r' = \lambda/\alpha$,

$$P_s(n) = e^{-r'} \frac{r'^n}{n!}, \quad n = 0, 1, \dots; \quad (2.14)$$

this is also obtained by letting $\mu \rightarrow 0$ in the above negative binomial probability generating function. Both results are consistent with the computations of §2.3, since $G_s(z) = \lim_{t \rightarrow \infty} G(z, t)$.

If either $\mu > 0$ or $\mu = 0$, a condition for existence of a stationary distribution is that $\alpha > \mu$: the rate at which beads disappear is lower than their rate of spontaneous appearance. For steady flow conditions, there are additional constraints on the parameters $\nu, \mu, \sigma, \lambda_0$, and λ_1 . On average, the number of particles that leave the observation window must match the number of particles that enter it,

$$\bar{N}\sigma + \bar{N}\nu = \lambda_0 + \lambda_1 + \bar{N}\mu, \quad (2.15)$$

where \bar{N} is the time-averaged number of particles. Moreover, bed equilibrium implies that on average, there is no variation in the bed elevation over time,

$$\bar{N}\sigma = \lambda_1 + \bar{N}\mu, \quad (2.16)$$

and that $\bar{N}\nu = \lambda_0$: the inflow matches the outflow.

To supplement our description of the statistical properties, we compute the autocorrelation function of the number of particles in motion within the window (Gardiner 1983),

$$\rho(\tau) = \frac{\mathbb{E}[(N(t+\tau) - \bar{N})(N(t) - \bar{N})]}{\text{Var}(N)} = \frac{\mathbb{E}[N(t+\tau)N(t)] - \bar{N}^2}{\text{Var}(N)},$$

where τ denotes the lag time and $\bar{N} = \mathbb{E}(N) = \lambda(\alpha - \mu)^{-1}$. For a statistically stationary process, there is no dependence on t , so this definition reduces to

$$\rho(\tau) = \frac{\mathbb{E}[N(\tau)N_0] - \bar{N}_0^2}{\text{Var}(N_0)}, \quad (2.17)$$

where N_0 is the initial number of particles within the control volume. The mean of $N(\tau)N_0$ can be expressed as

$$\mathbb{E}[N(\tau)N_0] = \sum_{n=0}^{\infty} \sum_{m=0}^{\infty} \text{Prob}(N = m, N_0 = n) nm = \mathbb{E}[N_0 \mathbb{E}(N(\tau) | N_0)],$$

in which the conditional mean of $N(\tau)$ given N_0 appears. This conditional mean can be obtained from equation (2.11) (Gardiner 1983),

$$\mathbb{E}(N(\tau) | N_0 = n) = \left(\frac{\partial G}{\partial z} \right)_{z=1} = nK + \lambda \frac{1-K}{\alpha - \mu},$$

and on substituting this into equation (2.17), we find that the autocorrelation function

is of exponential form

$$\rho(\tau) = e^{-\tau/t_c}, \quad (2.18)$$

where

$$t_c = \frac{1}{\alpha - \mu} > 0 \quad (2.19)$$

is the autocorrelation time.

2.5. Computation of the velocity of a single particle

We now use the energy balance equation to compute the velocity of a single rolling particle, which is assumed to reach a steady regime nearly instantaneously once set in motion (Ancey *et al.* 2003). On average, for steady flow conditions, the power supplied by gravity and fluid drag force is entirely dissipated by contact forces

$$m'g \sin(\theta \bar{u}_p) + \bar{P}_d = \bar{P}_c,$$

where $m' = m - 4\pi\rho_f a^3/3$ is the buoyant mass, $\bar{P}_d = \bar{\mathbf{F}}_d \cdot \bar{\mathbf{u}}_p$ is the power of drag forces supplied to the particle, where $\bar{\mathbf{F}}_d = C_d \pi a^2 |\mathbf{u}_f - \mathbf{u}_p|(\mathbf{u}_f - \mathbf{u}_p)$ is the drag force, with C_d the drag coefficient. The power P_c lost in contacts can be determined using results for a single bead rolling on a bumpy line in air. In this case, Ancey *et al.* (1996) have shown that dissipation can be broken into frictional and collisional parts

$$\bar{P}_c = \kappa_f m' g \bar{u}_p \cos \theta + \kappa_c \frac{\chi}{2a} m \bar{u}_p^3,$$

where $(2a)^{-1} \chi \bar{u}_p$ is the collision rate (if the bottom beads are regularly and closely arranged, then $\chi = 1$), $\kappa_c = 0.752$ reflects collisional dissipation, and $\kappa_f = 0.104$ is a bulk friction coefficient. The resulting equation of motion is a second-degree polynomial in \bar{u}_p ,

$$m'g \sin \theta + \frac{1}{2} \varepsilon C_d \pi a^2 \rho (\bar{u}_p - \bar{u}_f)^2 = \kappa_f m'g \cos \theta + \kappa_c \frac{\chi}{2a} m \bar{u}_p^2, \quad (2.20)$$

where $\varepsilon = +1$ when $\bar{u}_p < \bar{u}_f$ and $\varepsilon = -1$ when $\bar{u}_p > \bar{u}_f$. The single physical solution is

$$\bar{u}_p = k(Sh) \bar{u}_f, \quad (2.21)$$

where the factor $k(Sh)$ is given by

$$k(Sh) = \frac{1 - \sqrt{D_i}}{1 - 4\kappa_c \Delta \rho \chi / (3\varepsilon C_d)},$$

with

$$D_i = \frac{4}{9Sh} \frac{4\kappa_c \Delta \rho \cos \theta (\tan \theta - \kappa_f) + 3\varepsilon C_d (\kappa_c \Delta \rho \chi Sh - \cos \theta (\tan \theta - \kappa_f))}{C_d^2},$$

in which we have introduced the density ratio $\Delta \rho = \rho_p / \rho_f$. The parameter $k(Sh)$ is expressed as a function of the Shields number

$$Sh = \frac{\bar{u}_f^2}{2(\Delta \rho - 1)ag}. \quad (2.22)$$

The Shields number is generally defined as the ratio of the bottom shear stress to the equivalent in stress of a buoyant weight of the immersed particle [see equation (3.1)], but because of the relatively small submergence, we slightly modify this definition for the present purpose.

The particle usually moves more slowly than the fluid, but in certain circumstances—for instance on steep slopes—the opposite can occur. According to equation (2.20), the

condition $\bar{u}_p = \bar{u}_f$ yields $Sh_0 = \cos \theta (\tan \theta - \kappa_f) / (\kappa_c \chi \Delta \rho)$. When $Sh < Sh_0$, we have $\bar{u}_p < \bar{u}_f$ while for $Sh > Sh_0$, we have $\bar{u}_p > \bar{u}_f$; in that case, only gravity supplies energy to the particle while contact forces and water drag consume its energy. The latter condition holds only for slopes exceeding a critical value: $\theta > \theta_c = \arctan \kappa_f \approx 10\%$.

The previous analysis shows that the rolling regime has three sub-regimes of motion:

- for $\tan \theta < \kappa_f$, a solution is possible provided that the dimensionless number Sh exceeds a critical value

$$Sh_{cr} = 4 \cos \theta \frac{\kappa_f - \tan \theta}{3C_d}.$$

The value of Sh_{cr} may be determined by setting $\bar{u}_p = 0$ in equation (2.20). In this sub-regime, motion results mainly from the water action;

- for $\theta > \theta_c$ and $Sh < Sh_0$, the single physical solution is given by equation (2.21) with $\varepsilon = -1$. Motion results mainly from the action of gravity. However, such a solution is usually nonphysical since the condition $Sh < Sh_0$ also implies $h < 2a$; and
- for $\theta > \theta_c$ and $Sh > Sh_0$ the single physical solution is given by equation (2.21) with $\varepsilon = +1$. Motion results mainly from the combined action of water and gravity.

When the particle is in a saltating regime, analytical computation of the velocity is more delicate. Examples of computation have been given by a number of authors, including Yalin (1963), Gordon *et al.* (1972), Abbott & Francis (1977), Bridge & Dominic (1984), van Rijn (1985), Wiberg & Smith (1985), Niño & García (1994), and Ancey *et al.* (2002). To our knowledge, no analytic model provides realistic predictions of the trajectories and velocities of a saltating particle in water, because of the strong nonlinearities in the fluid forces exerted on the particle. This implies that numerical models should be used to derive particle velocity. The experimental results by contrast are surprisingly simple: it is mostly possible to derive linear or power-law relations between the velocities and the flow conditions such as Shields number and shear velocity (van Rijn 1985). Given the scope of this paper, it is best to use analytical albeit empirical expressions rather than numerical models. Earlier experimental investigation in our two-dimensional flume showed that the mean velocity of a single particle can be expressed as

$$\bar{u}_p = 3.2(\bar{u}_f - u_c), \quad (2.23)$$

with $u_c = 1.25 \tan^{1/2} \theta$ a critical velocity (Ancey *et al.* 2002).

Finally, note that it is possible to derive a single relation that holds for both rolling and saltating regimes (Ancey *et al.* 2003), but for the sake of simplicity, we do not develop this here.

2.6. Summary

Before addressing the validity of our approach by comparison with experiments, it is worth outlining its salient characteristics. For flows at equilibrium, we can compute the solid discharge as $\dot{n} = \sum_{i=1}^N u_i / L$. In the previous subsections, we have computed the number N of particles in motion and their individual velocity u_i , which is assumed to be directly linked to the fluid velocity through equations (2.21) and (2.23). We have shown that N is a random variable with the following properties:

- (a) its probability density is the negative binomial function (2.12) when particles are entrained both individually and collectively ($\mu > 0$), while it has the Poisson form (2.14) when collective entrainment does not occur ($\mu = 0$);
- (b) when $\mu > 0$, the variance must exceed the mean, while they are equal when $\mu = 0$, thereby providing a simple practical way to determine whether collective entrainment takes place;

(c) the autocorrelation function of N is the exponential function (2.18). As the particle velocity is not random, the solid discharge \dot{n} must have the same autocorrelation as N ;

(d) once moving, a particle continues for an exponential time, with parameter σ . The characteristic time (the mean duration of motion for one particle) is $t_{\sigma|1} = 1/\sigma$. The time for which it is stationary has a more complicated distribution. Since particles move independently, the mean deposition rate in a system of $N = n$ particles is $t_{\sigma|n}^{-1} = nt_{\sigma|1}^{-1} = n\sigma$; since the probability distribution of N is the negative binomial distribution given by equation (2.12), we deduce that the mean deposition rate is $t_{\sigma}^{-1} = \sum_{n=0}^{\infty} t_{\sigma|n}^{-1} \text{Prob}(n) = r(1-p)\sigma/p = \bar{N}\sigma$. The lag times must be distributed exponentially

$$\text{Prob}(\Delta t_{m \rightarrow b}) = \frac{1}{t_{\sigma}} e^{-\Delta t_{m \rightarrow b}/t_{\sigma}}. \quad (2.24)$$

The number of deposition events within a time interval δt can be computed similarly. The probability that a particle that moves at time t settles by time $t + \delta t$ is $p_d = 1 - \exp[-(\sigma + \nu)\delta t]$. Given that n particles are in motion at time t , the probability that k particles settle within the time interval $[t, t + \delta t)$ is then binomial with parameters n and p_d ; note that this holds true provided that δt is chosen long enough for several depositions to occur, but sufficiently short for the number of particles that start moving and then settle within the same interval to be zero. It follows that the unconditional probability of observing k particles that settle by δt is negative binomial with parameters r and $p' = p/(p + p_d - pp_d)$:

$$\begin{aligned} \text{Prob}(k \text{ depositions}; \delta t) &= \sum_{n=k}^{\infty} \text{Prob}(k \text{ depositions} \mid n; \delta t) \text{Prob}(n), \\ &= \sum_{n=k}^{\infty} \text{Bin}(k; n, p_d) \text{NegBin}(n; r, p) \\ &= \text{NegBin}(k; r, p'), \end{aligned} \quad (2.25)$$

since $\text{Prob}(n)$ is the negative binomial distribution (2.12) with parameters $r = \lambda/\mu$ and $p = 1 - \mu/\alpha$ when $\mu > 0$. When $\mu = 0$, the resulting distribution is Poissonian with parameter $r'' = p_d r$. Note that these expressions for the probability of observing k settling particles could have been used to derive the probability of waiting times—for instance by using the classical arguments to show the duality between Poisson and exponential distributions (Cox & Miller 1965)—and if we do so, we retrieve the result reported in equation (2.24).

(e) On average, the relative fraction of particles that cross the control volume \mathcal{V} without coming to rest is $\nu/(\sigma + \nu)$, while the fraction of particles that come to a stop is $\sigma/(\sigma + \nu)$.

(f) the entrainment coefficient λ_1 is expected to vary nonlinearly with the fluid velocity \bar{u}_f , but for narrow ranges of \bar{u}_f , the variation is almost linear;

(g) when flows are at equilibrium, the model parameters λ_1 , λ_0 , μ , ν , and σ must satisfy conditions (2.15) and (2.16). The autocorrelation time is given by equation (2.19). The ratio

$$\frac{t_c}{t_{\sigma|1}} = \frac{\sigma}{\sigma + \nu - \mu}$$

is lower than unity when there is no collective entrainment ($\mu = 0$), while it may exceed unity when there is collective entrainment ($\mu > 0$). Long range correlations are the consequence of collective entrainment (memory effect due to the coupling between entrainment and the number of moving particles); and

(*h*) the coefficients λ_1 , μ , and σ represent the entrainment and deposition rates within the control volume \mathcal{V} of length L . They are thus proportional to L .

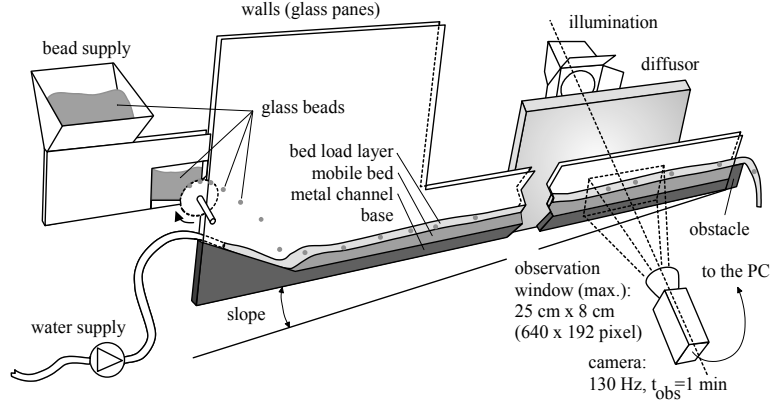


FIGURE 4. Sketch of the experimental setup.

3. Experimental setup and procedures

3.1. Overview

We conducted our experiments in a narrow flume (see §3.2). Sediment was replaced by glass beads of equal size. Our experimental facility is probably the simplest representation of bed load transport on the laboratory scale, with the advantages that boundary conditions are perfectly controlled and a wealth of information can be obtained using imaging techniques. Figure 4 shows a sketch of the experimental facility used. The nearly two-dimensional feature of this facility has some disadvantages: for instance, the low width-to-depth ratio leads to difficulties from the hydraulic point of view since turbulence may be controlled by the side walls rather than the bottom; and using spherical particles of the same size can be problematic in terms of bed arrangement, thus producing artificial conditions for particle entrainment. This was, however, the price paid for convenient access to the details of the flows.

We ran 15 experiments with different inclinations and various flow rates. Bed load equilibrium flows were achieved, i.e. neither erosion nor deposition of particles occurred on average, over sufficiently long time intervals. Figure 5 provides a snapshot of all experiments presented in this paper. Slopes and water discharges were selected so that we could record a sufficient number of events for our statistical analysis. The features of each run are summarized in Tables 1 and 2. The hydraulic conditions are specified using classic dimensionless numbers. The flow Reynolds number is defined as $Re = 4R_h\bar{u}_f/\nu_w$, where $R_h = Wh/(2h + W)$ denotes hydraulic radius, $\bar{u}_f = q_w/h$ the fluid velocity (averaged in the y - and z -directions), ν_w the kinematic viscosity of water, and h the time-averaged water depth. The Froude number $Fr = \bar{u}_f/\sqrt{gh}$ varied significantly over the experimental duration and along the main stream direction. The mean Fr values are reported in Tables 1–2. Although the mean Froude number exceeded unity, which means that the flows were supercritical on average, the instantaneous values of Fr fluctuated a great deal and frequent transitions to subcritical regimes occurred. This behaviour seems very close to that observed in gravel-bed rivers, where the Froude number is also found to fluctuate around the critical value (Grant 1997).

The solid concentration is defined as the ratio of the solid and the water discharges $C_s = q_s/q_w$. Values reported in Tables 1–2 are low, which indicates that particle flow was dilute. The ratio h/d is low, typically in the range 0.8–7. We used two definitions for the Shields number: the Shields number is classically defined as the ratio of the bottom

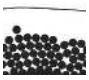
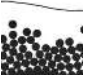
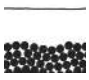


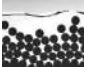
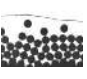
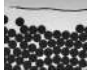
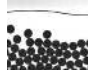
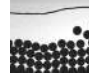
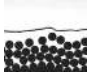
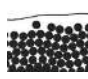
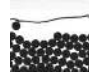
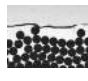
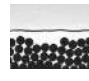
$\begin{matrix} \dot{n} \\ \text{(beads/s)} \\ \tan \theta \\ \text{(\%)} \end{matrix}$	6	7	8	9	11	16	21
7.5							
10							
12.5							
15							

FIGURE 5. Overview of the experiments conducted at various solid discharges \dot{n} and slopes $\tan \theta$. For each experiment, a detail of one filmed image is shown. See Tables 1 and 2 for the experimental conditions.

shear stress to the stress equivalent of a buoyant force (Julien 1994),

$$Sh = \frac{\rho g h \sin \theta}{(\rho_p - \rho_f) g a}, \quad (3.1)$$

and we also use the variant given by equation (2.22), which makes more sense for shallow flows. We report the mean particle velocities for the rolling (\bar{u}_r) and saltating regime (\bar{u}_s). We use $\kappa_{r/s} = N_r/(N_r + N_s)$ to refer to the number N_r of particles in a rolling regime relative to the total number of moving particles $N = N_r + N_s$.

3.2. Channel and material used

Experiments were performed in a tilted, narrow, glass-sided channel, 2 m in length and 20 cm in height. The channel width W was adjusted to 6.5 mm, which was slightly larger than the particle diameter ($2a = 6$ mm). In this way, particle motion was approximately two-dimensional and stayed in the focal plane of the camera. The channel slope $\tan \theta$ ranged from 5% to 15%, but only experiments within the slope range 7.5–15% are reported here.

The channel base consisted of half-cylinders of equal size (radius $r = 3$ mm) and randomly arranged on different levels. Disorder was essential, as it prevented slipping of entire layers of particles on the upper bed surface, which would have induced artificial erosion conditions. The effects of bed disorder were addressed by Böhm *et al.* (2004).

Colored spherical glass beads with a nominal diameter $2a$ of 6 mm and a density ρ_p of 2500 kg/m³ (provided by Sigmund Lindner GmbH, Germany) were used. They were injected from a reservoir into the channel using a wheel driven by a direct current motor and equipped with 20 hollows on the circumference, as depicted in Figure 4. For the experiments presented here, the injection rate \dot{n}_0 ranged from 5 to 21 beads per second, with an uncertainty of less than 5%. This corresponded to a solid discharge per unit width q_s/W of $9\text{--}38 \times 10^{-5}$ m²/s. The water supply at the channel entrance was controlled by an electromagnetic flow meter provided by Krohne (France). The discharge per unit width q_w ranged from 4 to 10×10^{-3} m²/s.

The hydraulic conditions (velocity profile, bed friction, etc.) have been specified in

TABLE 1. Flow characteristics and time-averaged values of dimensionless numbers characterizing bed load and water flow for $\tan \theta = 10\%$. Varying parameter: Solid discharge \dot{n} . The notation E10-6 means: $\tan \theta = 10\%$ and $\dot{n} \approx 6$ beads/s.

Experiment number	E10-6 (e)	E10-7 (f)	E10-8 (g)	E10-9 (h)	E10-16 (i)	E10-21 (j)
$\tan \theta$ (%)	10.0	10.0	10.0	10.0	10.0	10.0
\dot{n}_0 (beads/s)	5.3	6.7	8.0	10.0	15.4	20.0
q_w (10^{-3} m ² /s)	4.15	4.42	5.38	5.54	8.19	10.31
h (mm)	10.2	10.8	12.2	12.5	16.9	19.4
u_f (m/s)	0.41	0.41	0.44	0.44	0.48	0.53
\dot{n} (beads/s)	5.72	6.85	7.74	9.41	15.56	20.57
Re	4020	4090	4550	4570	5280	5910
Fr	1.42	1.37	1.38	1.36	1.24	1.26
Sh	0.95	0.95	1.10	1.10	1.30	1.59
Sh	0.113	0.120	0.135	0.139	0.188	0.216
C_s (%)	2.40	2.69	2.50	2.96	3.30	3.47
h/d	1.69	1.80	2.03	2.08	2.82	3.23
\bar{u}_r (m/s)	0.063	0.074	0.065	0.075	0.075	0.072
\bar{u}_s (m/s)	0.28	0.29	0.29	0.29	0.32	0.32
$\kappa_{r/s}$ (%)	43.9	38.9	41.6	43.2	41.2	43.7

TABLE 2. Flow characteristics and time-averaged values of dimensionless numbers characterizing bed load and water flow. The notation E7-6 indicates: $\tan \theta \approx 7\%$ and $\dot{n} \approx 6$ beads/s. See Tab. 1 for the experiments at $\tan \theta = 10\%$.

Experiment number	E7-6 (a)	E7-8 (b)	E7-9 (c)	E7-11 (d)	E12-9 (k)	E12-16 (l)	E12-21 (m)	E15-16 (n)	E15-21 (o)
$\tan \theta$ (%)	7.5	7.5	7.5	7.5	12.5	12.5	12.5	15.0	15.0
\dot{n}_0 (beads/s)	5.7	7.8	8.7	10.9	9.3	15.2	20.0	15.6	21.5
q_w (10^{-3} m ² /s)	10.00	11.54	13.85	26.15	2.97	3.85	4.46	2.31	2.92
h (mm)	18.9	20.8	24.9	40.8	7.0	8.2	9.4	4.9	6.7
σ_h (mm)	2.2	2.3	2.5	2.8	2.2	2.3	2.4	2.0	2.5
\bar{u}_f (m/s)	0.53	0.55	0.56	0.64	0.42	0.47	0.48	0.47	0.44
\dot{n} (beads/s)	5.45	7.76	9.20	10.99	9.52	15.52	19.86	15.45	20.55
Re	5860	6230	6400	7720	3760	4360	4600	3680	3830
Fr	1.26	1.26	1.15	1.02	2.20	2.09	1.90	3.72	2.63
Sh	0.158	0.173	0.207	0.340	0.098	0.114	0.130	0.082	0.111
Sh	1.59	1.71	1.78	2.32	1.00	1.25	1.30	1.25	1.10
C_s (%)	0.95	1.17	1.16	0.73	5.58	7.02	7.74	11.65	12.23
\bar{u}_r (m/s)	0.078	0.084	0.079	0.078	0.074	0.075	0.077	0.072	0.079
\bar{u}_s (m/s)	0.35	0.36	0.33	0.31	0.24	0.28	0.30	0.18	0.23
$\kappa_{r/s}$ (%)	31.2	30.3	33.3	32.4	78.4	72.6	63.9	95.1	82.2

earlier papers (Ancey *et al.* 2002; Böhm *et al.* 2004). Although the flume was narrow, its hydraulic characteristics were similar to those observed in wide channels with shallow flows.

3.3. Experimental procedures

The experimental procedure can be split into three major steps. First of all, a particle bed was built along the channel base, which remained stationary on average. To that end, an equilibrium between the water discharge, solid discharge, bed elevation, and channel slope was sought. This equilibrium was reached using the following procedure:

- (a) The water discharge q_w was set to a constant value.
- (b) An obstacle (approximately 20 mm in height) was positioned at the downstream end of the channel. The solid discharge \dot{n}_0 at the channel entrance (or the injection rate) was set to a constant value. The solid discharge q_s was calculated by the relation $q_s = \pi(2a)^3\dot{n}_0/6$. The first beads supplied by the feeding system were stopped by the obstacle at the channel outlet and started to form a bed. The bed line rose to the level of the obstacle and beads began to leave the channel. After approximately 10 minutes, the system arrived at bed-load equilibrium, i.e., there was no more bed deposition or erosion over a sufficiently long time interval.

(c) In order to make the bed line parallel with the channel base, the water discharge was then adjusted. After several iterations, we arrived at the configuration of a bed that consisted of two to three almost stationary bead layers along the channel, for which the bed line slope matched the channel base inclination. Average equilibrium conditions were sustained over long time periods, typically as long as 30 minutes.

Once bed equilibrium was reached, the particles and the water stream were filmed using a Pulnix partial scan video camera (progressive scan TM-6705AN), placed perpendicular to the glass panes at 115 cm away from the channel, approximately 80 cm upstream from the channel outlet. The camera was inclined at the same angle as the channel, behind which lights were positioned. An area of $L = 22.5$ cm in length and 8 cm in height was filmed and later reduced to accelerate image processing.

The camera resolution was 640×192 pixels for a frame rate of 129.2 fps (exposure time: 0.2 ms, 256 gray levels). Each sequence was limited to 8000 images due to limited computer memory; this corresponded to an observation duration of approximately 1 minute.

Images were analyzed using the WIMA software, provided by the *Traitement du Signal et Instrumentation* laboratory in Saint-Etienne (France). Positions of the bead mass centers were detected by means of an algorithm combining several image-processing operations; particle trajectories were calculated using a particle tracking algorithm (Böhm *et al.* 2006).

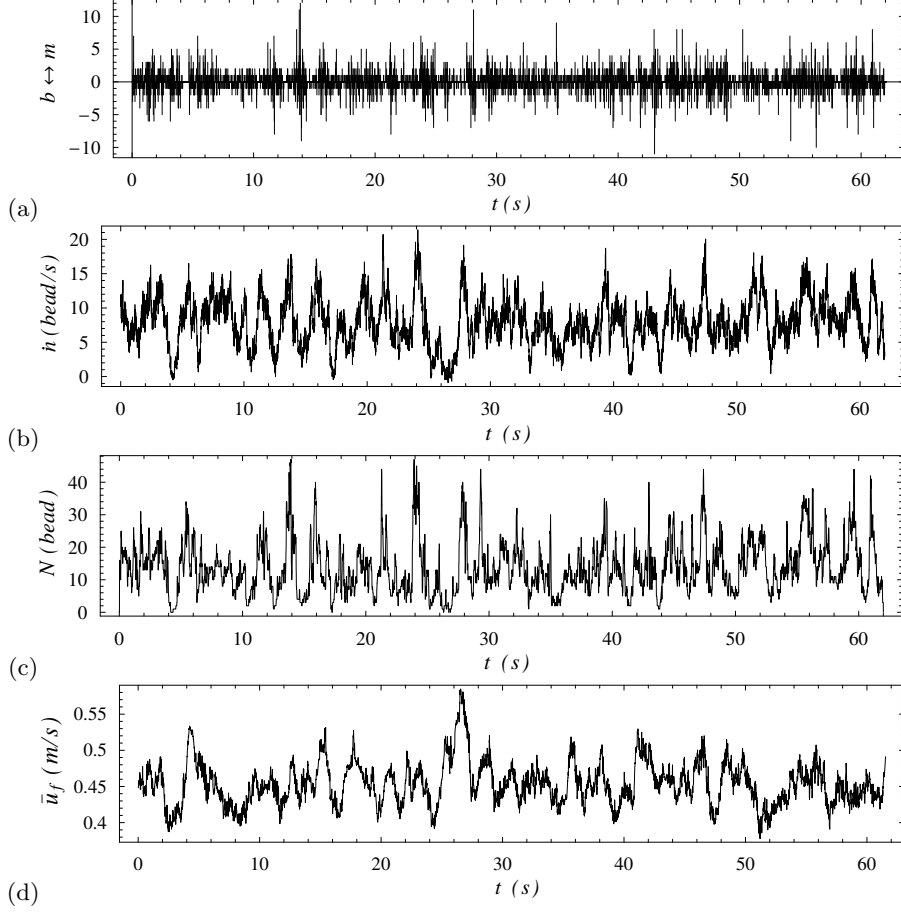


FIGURE 6. Experiment (g) E10-8. (a) particle exchanges between the bed and the flow: each bar oriented upward indicates the number of beads that passed from the resting state to the rolling regime over a given time interval $\delta t \approx 1/130$ s; downward-oriented bars represent the number of rolling particles coming to a halt. (b) Solid discharge \dot{n} as a function of time. (c) Variation in the number of moving particles N . (d) Mean fluid velocity \bar{u}_f as a function of time.

4. Experimental results

With our experimental facility, we can probe quantities such as the number of particles that come to a halt or are entrained for some time interval. Figure 6 shows typical records for four variables of interest: the number of particles passing from a resting to a moving state ($b \rightarrow m$) and conversely ($m \rightarrow b$) as a function of time; the time variations in the solid discharge \dot{n} ; the number of moving particles N ; and the fluid velocity \bar{u}_f . These results were obtained for a mean bed slope of 0.1 and a solid discharge at the flume inlet $\dot{n}_0 = 8$ beads/s (experiment 10-8 in Table 1); the plots are typical of those results for other solid discharges \dot{n}_0 and slopes.

Figure 7 shows the variations in the solid discharge \dot{n} as a function of the mean fluid velocity \bar{u}_f . Like most laboratory experiments conducted with low water discharges, the solid discharge varies nearly linearly with the mean fluid velocity. A similar dependence is found if we replace \bar{u}_f with the fluid discharge or the Shields number. The range of \bar{u}_f (0.41–0.64 m/s) was, however, not sufficiently wide to claim that the relation $\dot{n}(\bar{u}_f)$ or q_w was linear. Note the significant increase in the solid discharge when the bed slope

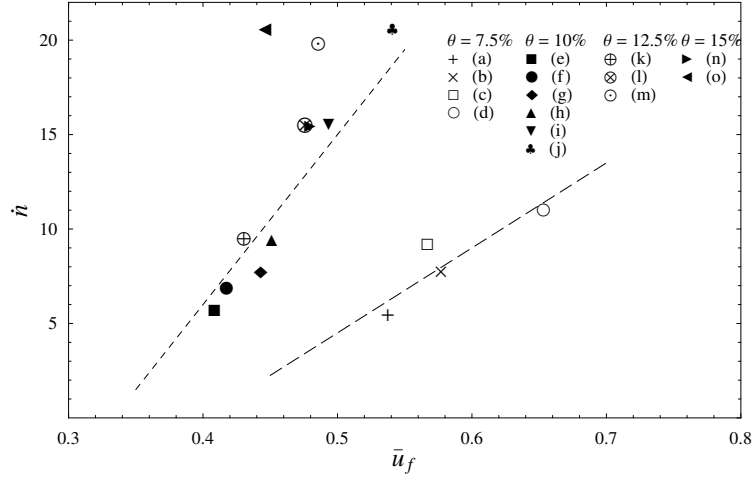


FIGURE 7. Variation in \dot{n} with \bar{u}_f . The dashed lines represent empirical trends adjusted on the data: $\dot{n} = 90\bar{u}_f - 30$ (dashed line) for $\tan \theta = 0.1 - 0.125$ and $\dot{n} = 45\bar{u}_f - 18$ (long dashed line) for $\tan \theta = 0.075$.

is increased from 7.5% to 10%, and the small changes when the slope is increased from 10% to 12.5%. The strong dependence of solid discharge on channel inclination and the linearity with water flow rate are reflected by many empirical formulas. For instance, Rickenmann (2001) deduced from flume experiments that $q_s \propto \tan^2(\theta(q_w - q_c))$, with q_c a critical water discharge corresponding to incipient motion. Incidentally, note that here, for the sake of simplicity, no correcting factor was applied to take into account sidewall effects, as usually done in hydraulics for narrow channels; if we correct the influence of sidewalls on the mean fluid velocity by using the hydraulic radius rather than the flow depth, we obtain a smoother variation in \dot{n} with bed slope (Frey *et al.* 2006).

Below we assess the reliability of our model by comparing its predictions with our experimental data. As the model is not closed, we need to estimate some of its parameters, which biases comparison to some degree. In § 4.1 we outline how we determine the unknown parameters. In § 4.2 we analyse the probability distribution and the autocorrelation function of the number of moving particles. Although there is good agreement between theory and experiments as regards the probability distribution function of N , there is an appreciable difference for the autocorrelation time t_c , perhaps as a consequence of collective effects when particles come to rest (§ 4.3). In § 4.4, we investigate the dependence of the entrainment rates on the mean fluid velocity. A striking result emerges in the analysis of the mean particle velocity (§ 4.5): we show that \bar{u}_p exhibits little dependence on \bar{u}_f , which contrasts with physical intuition and theoretical analysis (§ 2.5). Finally, in § 4.6, we try to estimate the different sinks of energy for flows at equilibrium.

4.1. Parameter estimation

A classic impediment to any approach to sediment transport is that the models contain parameters that cannot be computed analytically, because they are empirical or represent complex processes whose description requires heavy computation. Our model does not disprove this rule. It involves eight variables: the number of moving particles N , the mean particle velocity \bar{u}_p , the solid discharge \dot{n} , the inflow rate λ_0 , the entrainment rate of individual particles λ_1 , the collective entrainment rate μ , the deposition rate σ , and the outflow rate ν . The fluid discharge q_w and the channel slope θ are control parameters of our experiments. These variables are not independent (see § 2.6), as we have found

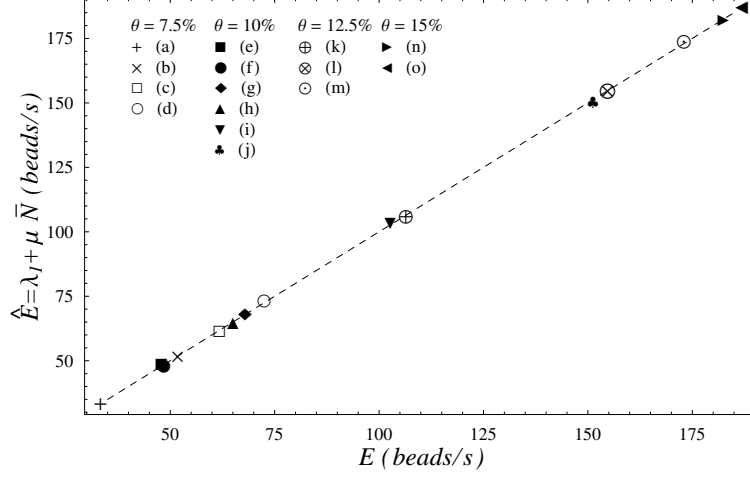


FIGURE 8. Comparison between the measured entrainment rate E and estimated value $\hat{E} = \lambda_1 + \mu \bar{N}$. The dashed line represents the first bisectrix.

five relationships among the eight parameters related to the solid discharge; thus we would need three additional relations to close our system. Here, the closure equations are replaced with data fitting on three variables. Since we tuned the solid flow rate at the channel entrance for the flow to be at equilibrium, we consider that the flow rate and the number of particles are prescribed. Moreover, we can measure the settling rate to deduce σ . This provides us with the three required additional equations. We therefore assume below that λ_0 , N , and σ are prescribed at the channel inlet or measured within the control volume. Indeed, from the record $N(t)$, we infer the mean and the variance, \bar{N} and $\text{Var}N$, respectively. The deposition rate σ was computed as the ratio of the total number of particles deposited to the experiment duration (approximately 1 minute).

We can then estimate the coefficients μ , ν , and λ_1 using equation (2.13) and the equilibrium conditions (2.15)–(2.16), yielding

$$\mu = \lambda_0 \left(\frac{1}{\bar{N}} - \frac{1}{\text{Var}N} \right) + \sigma \left(1 - \frac{\bar{N}}{\text{Var}N} \right), \quad \lambda_1 = (\lambda_0 - \bar{N}\sigma) \frac{\bar{N}}{\text{Var}N} - \lambda_0, \quad \text{and} \quad \bar{N}\nu = \lambda_0. \quad (4.1)$$

The autocorrelation time \hat{t}_c of $\dot{n}(t)$ and $N(t)$ is given by equation (2.19). In practice, the autocorrelation function was estimated by taking the Fourier transform of $N(t)$

$$\hat{\rho} = \mathcal{F}^{-1}(\mathcal{F}(N)\mathcal{F}(N)^*),$$

where \mathcal{F} denotes the Fourier transform, $\mathcal{F}(N)^*$ is the complex conjugate of $\mathcal{F}(N)$, and \mathcal{F}^{-1} denotes the inverse Fourier transform. Another way to estimate the autocorrelation time is to fit the exponential form (2.18) directly to the data to estimate the experimental correlation time \hat{t}_c . The estimate depended on the number of observations used to fit the exponential function. For instance, for experiment (g) E10-8, we obtained $\hat{t}_c = 0.283$ s when taking the first 50 data against $\hat{t}_c = 0.243$ s when a row of 100 data was used. The empirical autocorrelation function may become negative.

The parameter estimates are reported in Table 3. Figure 8 shows the measured entrainment rate E and its estimated value $\hat{E} = \bar{N}\mu + \lambda_1$, computed from the estimates of μ and λ_1 . The perfect match confirms that the flows were at equilibrium; \hat{E} was in fact obtained from the measurement of the settling rate σ using equation (4.1).

TABLE 3. Measured values of the total number of particles moving within the window (mean values \bar{N} and variances $\text{Var}(N)$), autocorrelation times \hat{t}_c computed using equation (2.19), autocorrelation times \tilde{t}_c estimated by fitting an exponential curve to the data, and inferred values of the model parameters obtained using equation (4.1). Times in s, rates in beads/s.

No.	\bar{N}	$\text{Var}(N)$	\hat{t}_c	\tilde{t}_c	λ_0	λ_1	ν	σ	μ
(a)	7.06	22.53	0.59	0.36	5.45	6.59	0.77	4.67	3.74
(b)	9.83	30.94	0.52	0.27	7.76	11.21	0.79	5.28	4.14
(c)	12.19	35.43	0.50	0.29	9.20	15.14	0.75	5.05	3.81
(d)	14.86	38.51	0.46	0.23	10.99	21.40	0.74	4.91	3.47
(e)	9.46	70.74	1.30	0.37	5.72	1.53	0.60	5.13	4.96
(f)	9.86	36.89	0.67	0.36	6.85	7.80	0.69	4.86	4.07
(g)	13.76	64.55	0.85	0.24	7.74	8.42	0.56	4.95	4.34
(h)	13.67	49.09	0.66	0.33	9.41	11.24	0.69	4.74	3.91
(i)	22.83	72.09	0.61	0.21	15.56	22.07	0.68	4.52	3.56
(j)	34.21	128.91	0.75	0.17	20.57	24.78	0.60	4.39	3.67
(k)	21.89	123.38	1.07	0.26	9.52	10.96	0.43	4.84	4.34
(l)	32.39	182.68	1.07	0.20	15.52	14.64	0.48	4.77	4.32
(m)	38.52	222.88	1.15	0.23	19.86	13.62	0.52	4.51	4.16
(n)	43.31	214.31	1.08	0.17	15.45	24.49	0.36	4.21	3.64
(o)	47.86	130.06	0.63	0.12	20.55	55.72	0.43	3.90	2.74

4.2. Number of moving particles

Figure 9 shows the probability density function of N for experiments (a)–(o). The dots represent the empirical probabilities, while the dashed line stands for the negative binomial distribution (2.12), the parameters of which were estimated using the measured values $\text{Var}N$ and \bar{N} reported in Table 3; for the sake of readability, we plotted the discrete probability mass functions as continuous curves.

First note the fairly good agreement between the data and theoretical probability distribution for all experiments. Local departures and data scattering are seen, but they are usually associated with low probabilities. Since 8'000 data were used for each run, empirical probabilities lower than 10^{-3} are unimportant. Deviations are also visible at $N = 0$. In that case, it should be kept in mind that from the algorithmic point of view, it was difficult to discriminate the instances in which a particle was really set in motion from those in which a bed particle just swung around its rest position (Böhm *et al.* 2006), which might introduce slight errors when counting the number of moving particles. The plots confirm that the negative binomial distribution is a good candidate for describing the statistical behaviour of N over a wide range of flow conditions. If we set $\mu = 0$ (Einstein-like theory), the theoretical distribution is no longer the negative binomial distribution (2.12), but the Poisson distribution (2.14), whose variance and mean are equal. This supports the idea of collective entrainment or, at least, does not undermine the simple assumption used for modelling entrainment.

There is a significant change in the distribution shape when the water discharge increases. When it is low [e.g., panel (e) in Figure 9], the empirical distribution is close to a straight line on a logarithmic scale, implying that the number of particles decays exponentially within the observation window. For experiment (e), the discrepancy between empirical and theoretical probability distributions is the most pronounced of all runs, which may mean that theory performs less well for these discharges (as expected, see § 2.2). With increasing water discharge, the probability distribution takes a bell shape, which is first skewed, then nearly symmetric at the highest slopes and flow rates [see panel

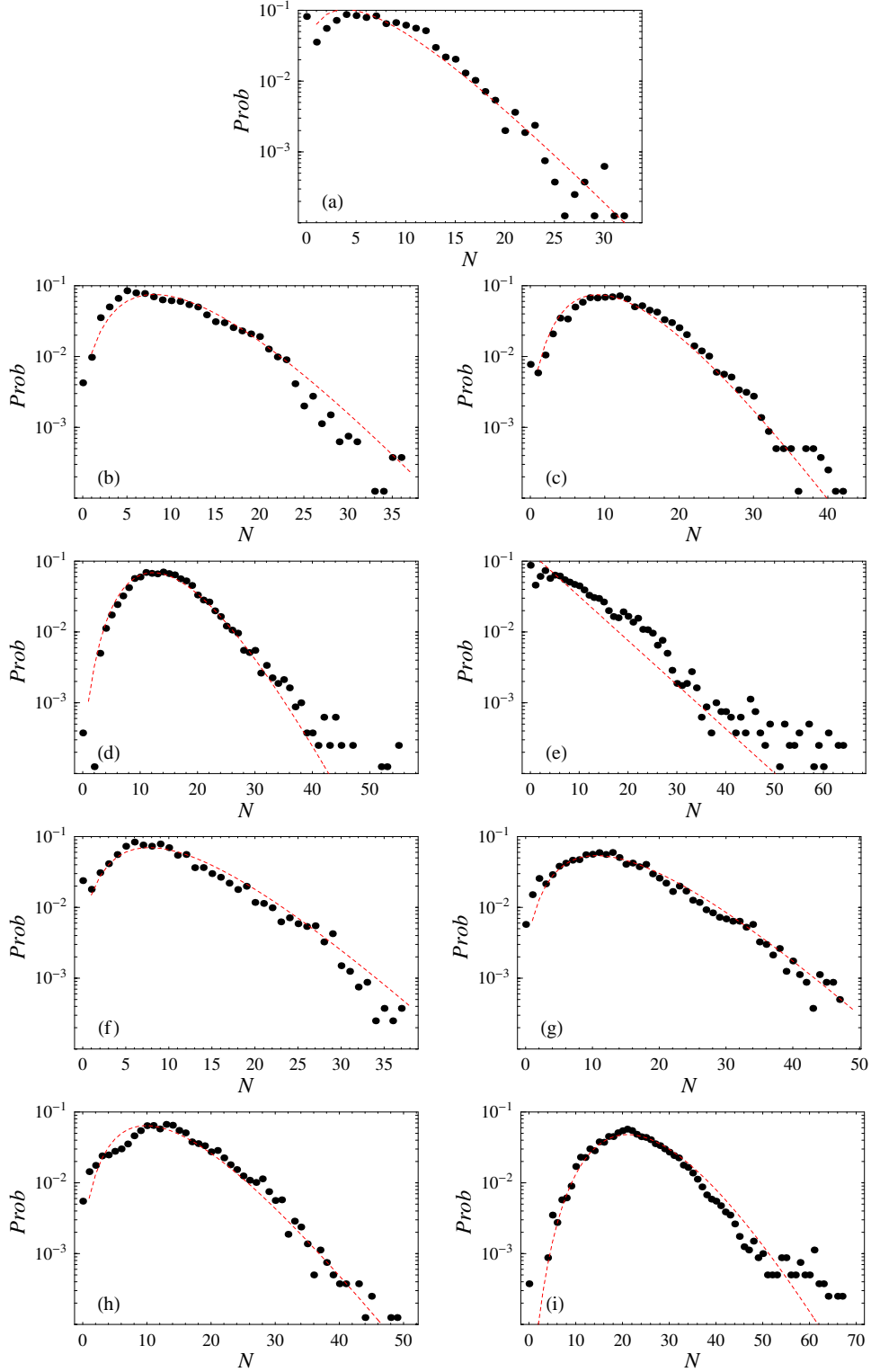


FIGURE 9. Empirical probability density of the total number of moving beads N (black dots). The dashed line is the probability density function of the negative binomial distribution. Experiments (a-i).

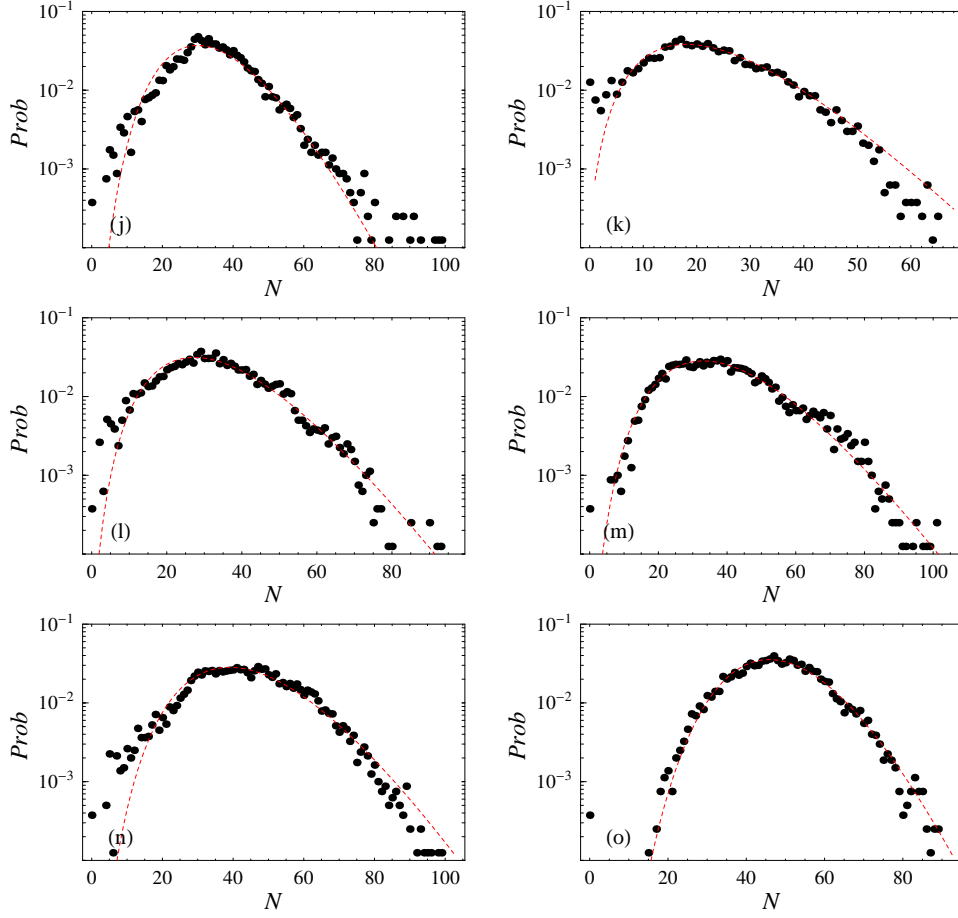


FIGURE 9. (Continued). Empirical probability distribution of the total number of moving beads N (black dots). The dashed line is the probability density function of the negative binomial distribution. Experiments (j–o).

(o) of Figure 9]. In the case of run (o), the discrete empirical probability distribution can be approximated by a Gaussian distribution.

For each run, the sample variance exceeded the mean, but the ratio $\text{Var}N/\bar{N}$ decreased with increasing water discharge (or Shields number). For instance, for slope $\tan \theta = 0.1$, the ratio $\text{Var}N/\bar{N}$ was as high as 7 for run (e) and dropped to below 3 for run (j). Thus for each run, the number of moving particles varied frequently and widely, but with increasing water discharges, wide fluctuations became less frequent, which substantiates the idea that at high water discharges, sediment transport becomes more continuous.

Figure 10 shows the autocorrelation functions of the total solid discharge, the number of moving beads, and the theoretical curve (2.19), where the autocorrelation time t_c is replaced by its estimate \hat{t}_c given by equation (4.1). The striking point is that the autocorrelation functions $\bar{\rho}$ for the solid discharge and the number of moving particles are quite similar for each run, as theoretically expected (see § 2.6), which shows that the instantaneous particle velocities were never too far their mean values. The behaviour of $\bar{\rho}$ at short times is nearly exponential, as expected, but the theoretical autocorrelation time \hat{t}_c is much longer than the experimental value t_c . The values of \hat{t}_c and t_c given in Table 3 show that \hat{t}_c/t_c ranges from 1.6 to 6.3, with a mean value of 3.5. We shall see

that to a large extent, this discrepancy stems from the statistical behaviour of deposition events (see §4.3), which are more frequent than theoretically computed, but of smaller amplitude.

Despite this shortcoming of the theoretical model, the salient features of solid-discharge fluctuations are correctly described, notably the ratio t_c/t_σ (see §2.6) ranges from 2 to 9, which shows that the solid discharge exhibited long-range fluctuations, the durations of which are much longer than the typical timescale associated with particle motion. Figure 11 shows the autocorrelation functions for the number of moving particles N , the solid discharge \dot{n} , the mean fluid velocity \bar{u}_f , the bed elevation, and the theoretical number of particles for run (g). The theoretical curve lies midway between the autocorrelation curves for the bed elevation and mean fluid velocity. The solid discharge is associated with the shortest autocorrelation time. The autocorrelation function of \bar{u}_f may be questionable since for a turbulent flow, we would expect shorter autocorrelation times, but one must recall that \bar{u}_f is the mean velocity within the entire window, that is, \bar{u}_f is a double averaged velocity (in time and space), which explains why fastest fluctuations were dampened out.

4.3. Deposition rate

Another interesting aspect of our experiments is the deposition rate of moving particles. From time series such as that in Figure 6(a), we can compute the lag times $\Delta t_{b \rightarrow m}$ between two deposition events within the observation window. We can then infer the statistical properties of the lag times $\Delta t_{b \rightarrow m}$. Figure 12 reports the empirical probability distribution of $\Delta t_{b \rightarrow m}$ for runs (a)–(o). On the same figures, we have plotted the theoretical curve given by equation (2.24), which is an exponential density with parameter $t_\sigma^{-1} = (1-p)r\sigma/p = \bar{N}\sigma$. As in §4.2, given the size of our samples, the empirical probabilities make sense only when they are in excess of 10^{-3} ; moreover, since the acquisition rate was approximately 130 Hz, we could not resolve events that occurred within time intervals shorter than 10 ms.

For low flow rates and gentle slopes ($\tan \theta \leq 0.1$), the theoretical probability distribution provides a crude approximation to the empirical distribution (runs a–i): while the shape of the empirical distribution is well captured (exponential behaviour), the deviation between the theoretical and empirical curves suggests that the mean lag time is longer than predicted. At higher flow rates or steep slopes, the model yields even cruder approximations, but still captures the main trend. The deviation between theoretical and experimental curves is more pronounced for experiments conducted at $\tan \theta = 0.15$. Figure 13 compares the expected mean lag time t_σ with the mean of the experimental samples $\Delta \bar{t}_{mb}$. On the whole, the agreement is good, but a closer look shows that the mean experimental lag time is twice the expected value t_σ : deposition events occur more frequently empirically than assumed with our model.

If we plot the probability of observing $n_{m \rightarrow b}$ particles settling during a time interval $\delta t = 1/130$ s, there are less substantial differences between the theoretical and empirical distributions. Figure 14 shows these probability distributions for runs (a)–(o). Theoretically, the number of settling particles follows the probability distribution (2.25) derived in §2.6. The behaviour at low $n_{m \rightarrow b}$ values is well captured by the theoretical curve: for all slopes and flow rates, the data fall onto the theoretical curve, for $n_{m \rightarrow b}$ as large as 3 to 6. For larger $n_{m \rightarrow b}$ values, there are significant deviations between data and predictions. Experimentally, we observe an exponential decay of the number of settling particles, which shows that occasionally, a group of several particles (up to 12–14 particles at the steepest slopes) can come to rest. The exponential decay is observed for all slopes and

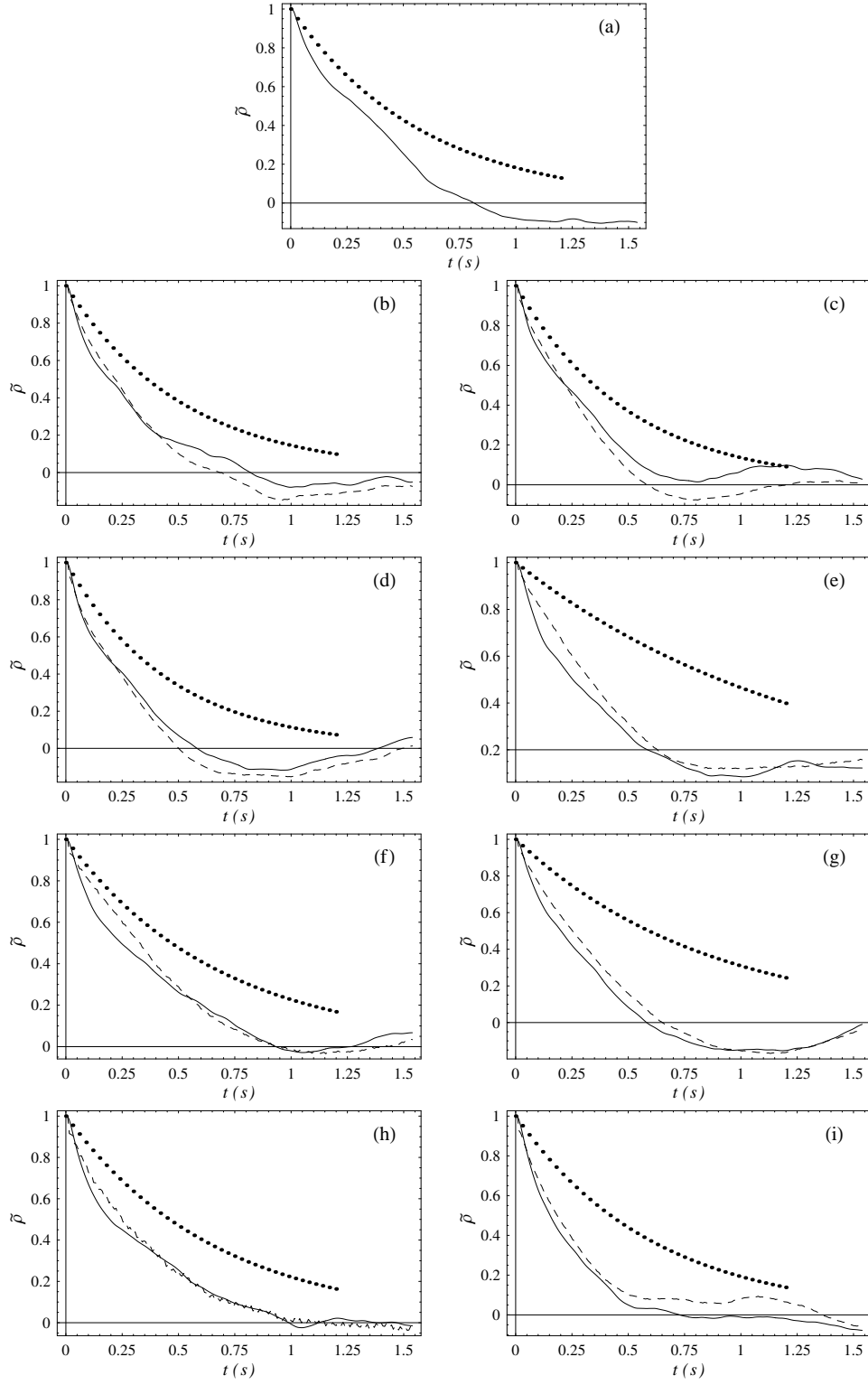


FIGURE 10. Autocorrelation functions of the number of moving beads (solid line) and the solid discharge (dashed lines). Dotted lines stand for the theoretical autocorrelation function (2.19), when the autocorrelation time \hat{t}_c is evaluated using equation (4.1). Experiments (a-i).

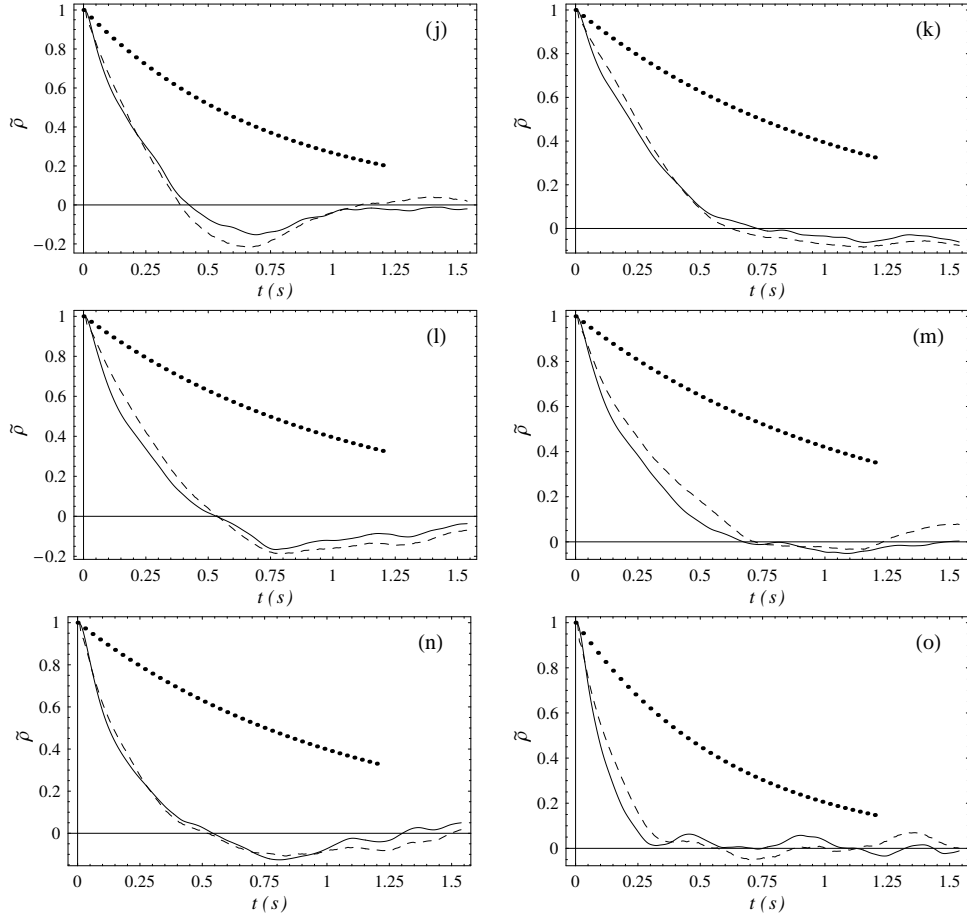


FIGURE 10. (Continued). Autocorrelation functions of the number of moving beads (solid line) and the solid discharge (dashed lines). Dotted lines stand for the theoretical autocorrelation function (2.19), when the autocorrelation time \hat{t}_c is evaluated using equation (4.1). Experiments (j–o).

discharges. The theoretical probability also entails exponential decay, but its decay rate is much larger (by a factor or roughly ten) than the empirical rate.

In conclusion, we observe empirically that deposition occurs a little less frequently and the number of deposited particles over short time intervals can be much larger than expected with our model. This higher activity contributes to decreasing the autocorrelation time t_c of the solid discharge, which may explain why we only found the order of magnitude of t_c . Note also that Table 3 shows little correlation between the deposition rate σ and the fluid velocity \bar{u}_f , which may suggest that σ is a constant parameter.

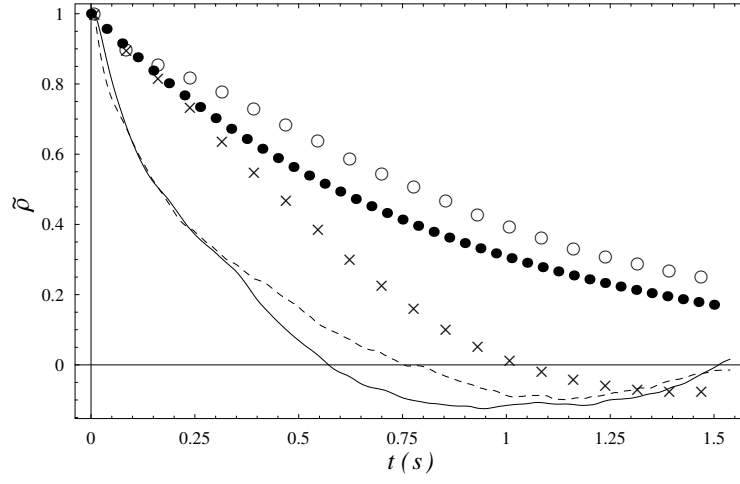


FIGURE 11. Autocorrelation functions of the number of moving particles (solid line), solid discharge (dashed line), mean fluid velocity (crosses \times), bed elevation (empty circles \circ), and theoretical autocorrelation functions (dotted line), given by equation (2.19). Data from run (g) E10-8.

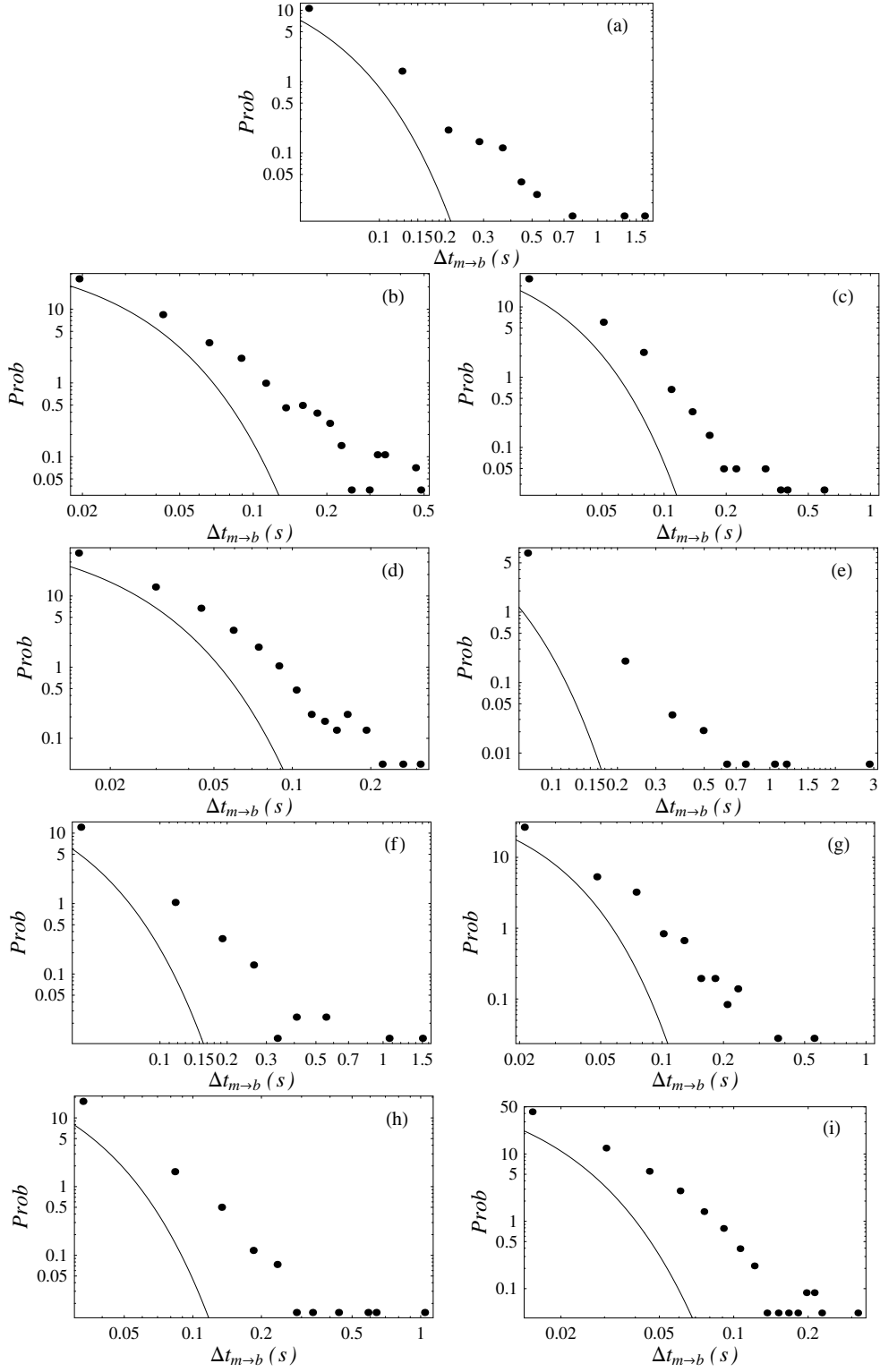


FIGURE 12. Probability distribution of lag times: dots represent empirical probabilities, while the solid line stands for the theoretical curve (2.24). Experiments (a–i).

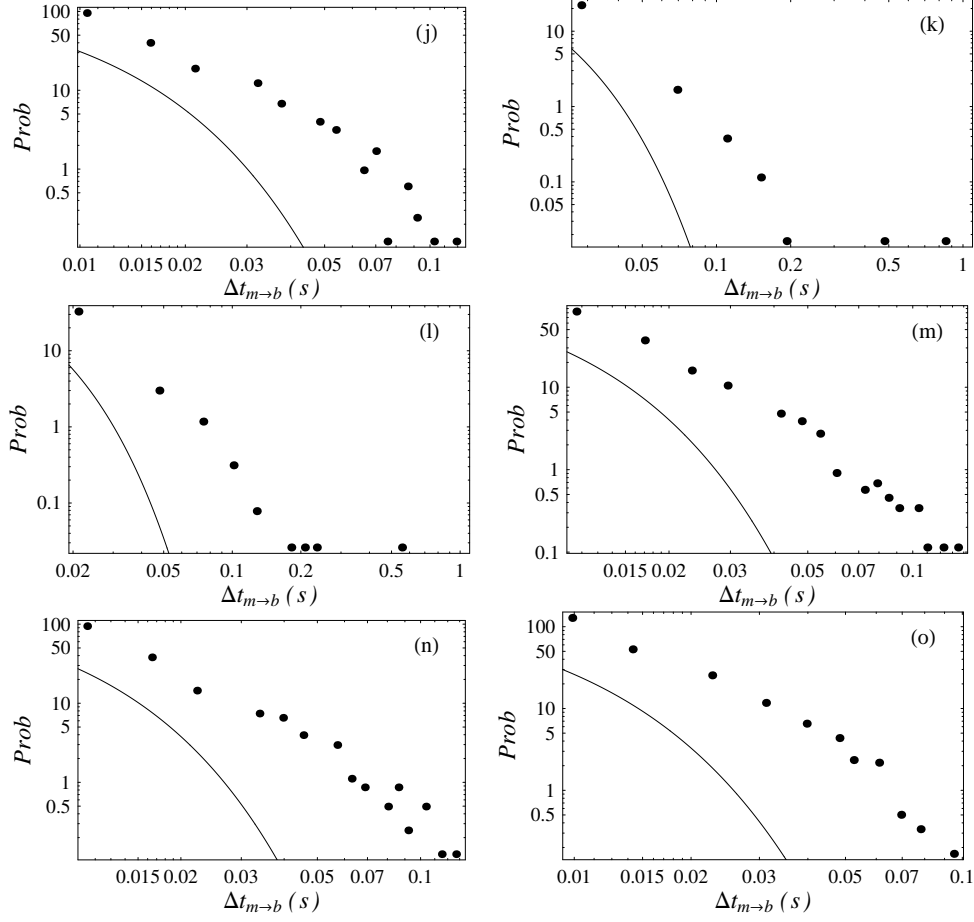
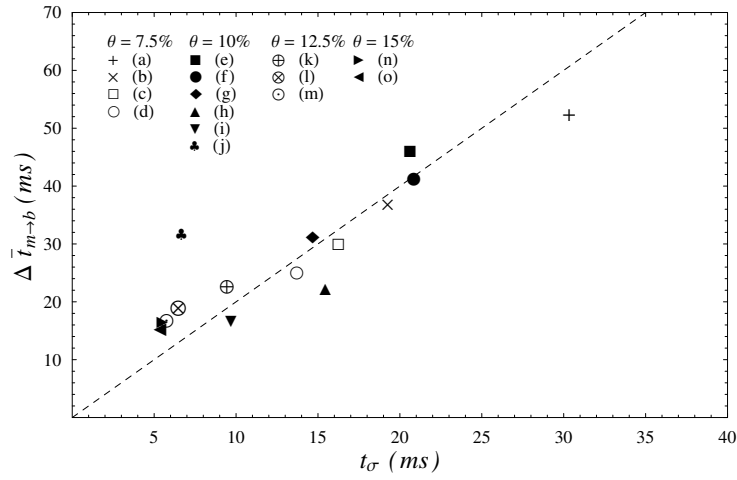


FIGURE 12. (Continued). Experiments (j–o).

FIGURE 13. Comparison between the mean experimental lag time $\Delta \bar{t}_{mb}$ and the theoretical value $t_\sigma = 1/(\bar{N}\sigma)$. The dashed line stands for the empirical trend $\Delta \bar{t}_{mb} = 2t_\sigma$.

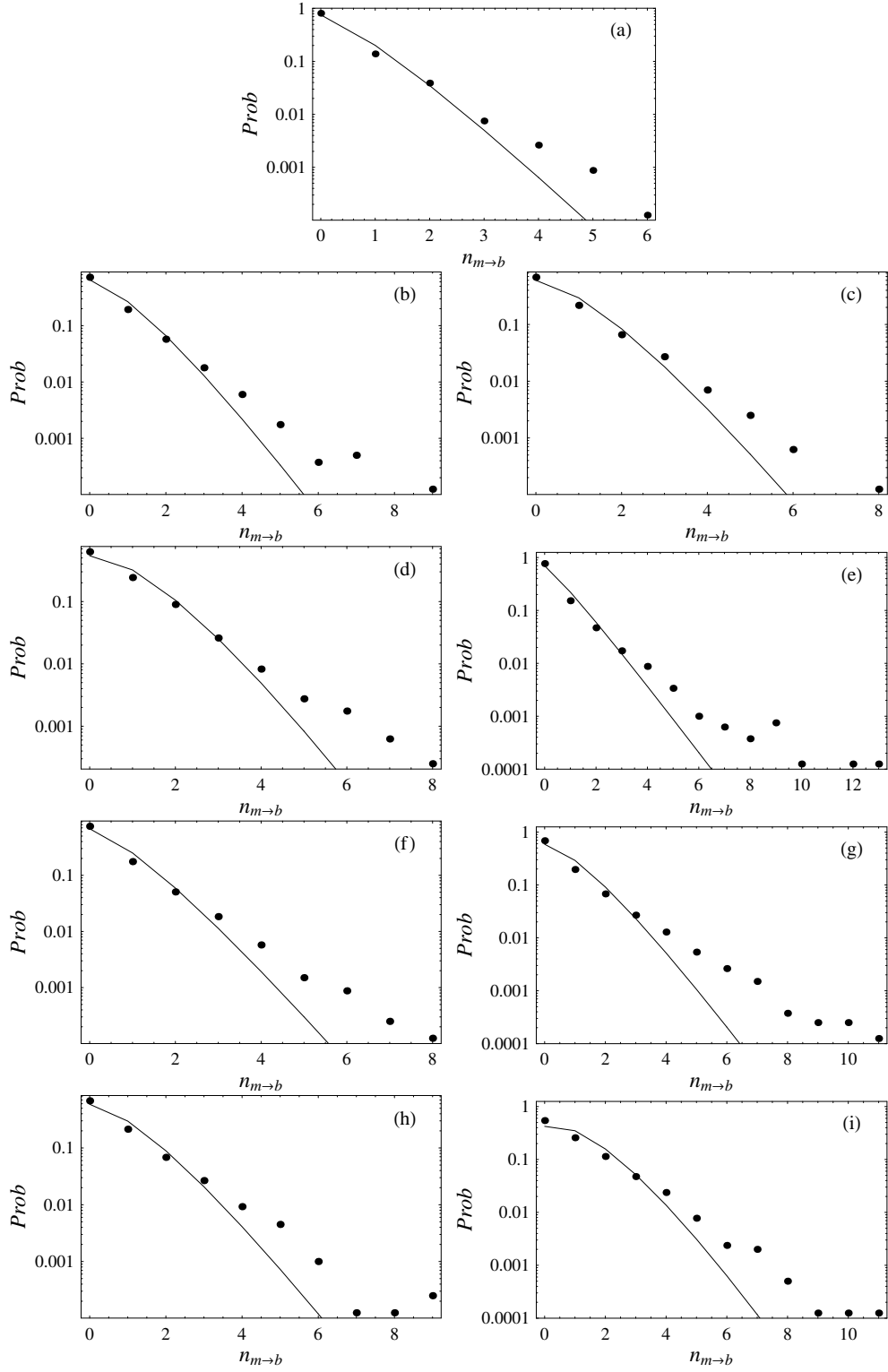


FIGURE 14. Probability distribution of the number of particles that come to a halt during a time interval δ : dots represent empirical probabilities, while the dashed line represents the theoretical distribution (2.25). Experiments (a-i).

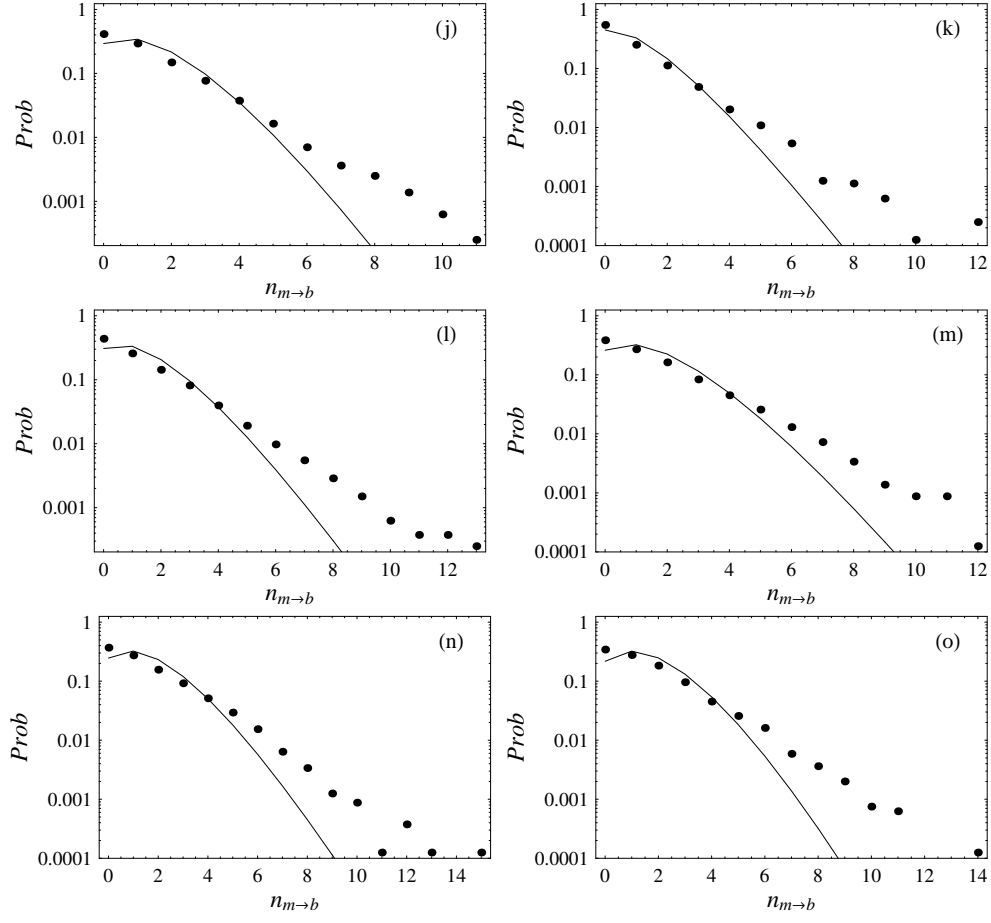


FIGURE 14. (Continued). Experiments (j–o).

4.4. Entrainment rates

Figure 15 shows how the entrainment rates λ_1 and μ vary with the mean fluid velocity \bar{u}_f and how λ_0 is related to λ_1 . Figure 15(a) reveals a linear relation between the inflow coefficient λ_0 and the entrainment rate λ_1 for the gentlest slopes and lowest flow rates ($\tan \theta \leq 0.1$ and $\dot{n} < 16$ beads/s). At higher flow rates or for steep slopes, there is no clear trend, but this may stem from the dearth of data. At very low entrainment rates, the influx coefficient λ_0 is much higher than λ_1 , suggesting that bed load transport can take place with little entrainment of isolated particles.

Figure 15(b) shows that the entrainment rate λ_1 grows with increasing fluid velocity. There is no very clear trend, but it appears that the data related to slopes $\tan \theta = 0.1$ and $\tan \theta = 0.125$ collapse onto a single straight line, while the data corresponding to $\tan \theta = 0.075$ form a parallel line. This closely reflects the behaviour observed for the solid discharges in Figure 7, with the same reservation about the role of sidewalls. This strong dependence on slope suggests that theoretical analysis of incipient motion on sloping beds, which provides weak dependence on $\cos \theta$, underestimates the influence of bed slope on entrainment. The linear variation in λ_1 with \bar{u}_f is consistent with the heuristic arguments presented in § 2.2. The estimated waiting time given by equation (2.7) is around 50 ms if we take the typical values $P_c = 0.5$, $L_x \sim h = 2$ cm, and $\langle u \rangle \sim \bar{u}_f = 50$ cm/s, consistent with the mean lag time values reported in Figure 13 (since $\Delta t_{m \rightarrow b} \approx \Delta t_{b \rightarrow m}$ in a steady state). For the highest bed slope $\tan \theta = 0.15$, we observe a drop in the entrainment rate with increasing fluid velocity, which is probably directly linked to the very low flow submergence conditions for this slope.

Figure 15(c) shows that the collective entrainment coefficient μ decreases nearly linearly with increasing fluid velocity, but this decay rate is very low since it passes from 4 beads/s to 3 beads/s when the mean fluid velocity is increased from 0.4 to 0.65 m/s. It may be reasonable to consider it as a constant parameter.

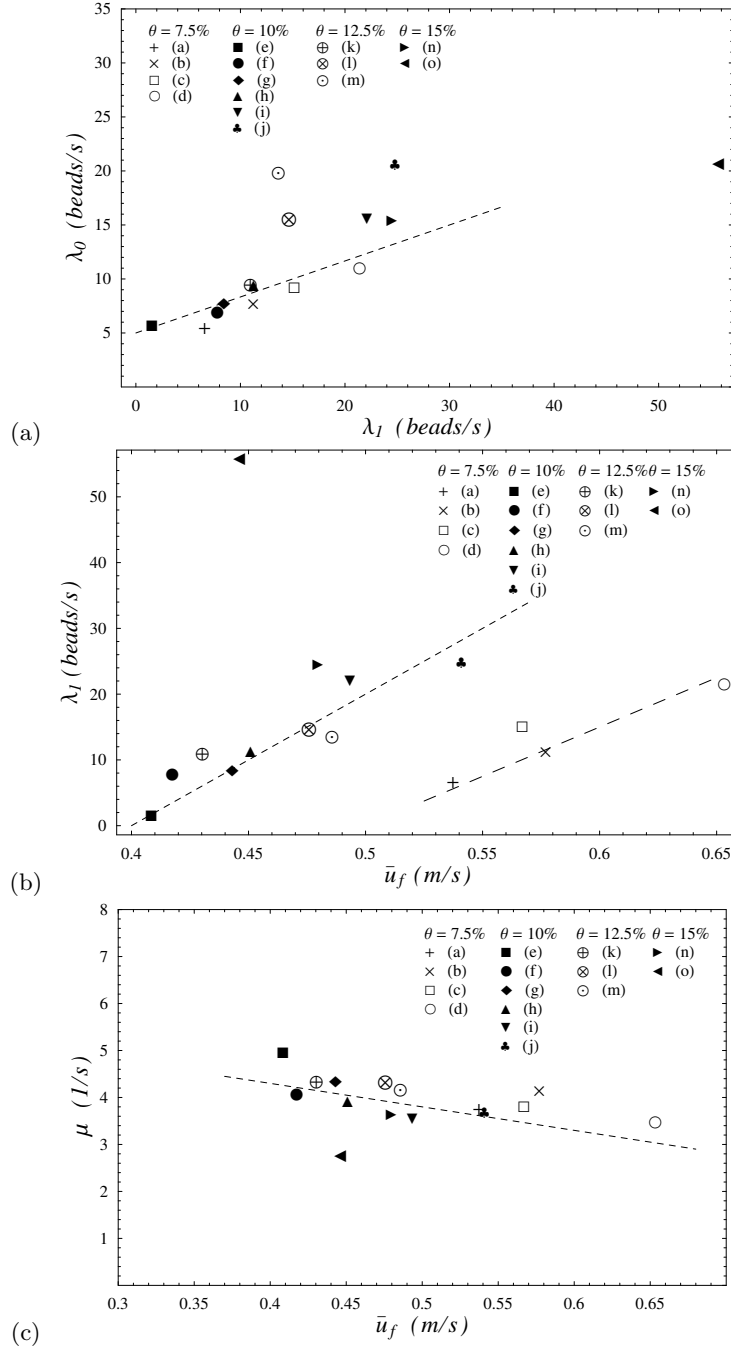


FIGURE 15. (a) λ_0 as a function of λ_1 ; the dashed line represents the experimental trend $\lambda_0 = 5 + \lambda_1/3 + 5$. (b) Entrainment rate λ_1 as a function of the mean fluid velocity; the dashed line represents the experimental trend $\lambda_1 = 200(\bar{u}_f - 0.4)$ for slopes $\tan \theta \geq 0.1$, while the long-dashed line stands for the experimental trend $\lambda_1 = 150(\bar{u}_f - 0.5)$. (c) Entrainment rate μ as a function of the mean fluid velocity; the dashed line represents the experimental trend $\mu = 2.3 - 5\bar{u}_f$.

4.5. Particle velocity

Figure 16 shows how the mean particle velocity varies with fluid velocity for particles in a rolling regime [Figure 16(a)] or in a saltating regime [Figure 16(b)]. It is striking that the mean velocity \bar{u}_r of rolling particles is almost independent of fluid velocity in our experiments, while theoretically we obtained a nonlinear increase in \bar{u}_r with \bar{u}_f (see § 2.5) in full agreement with earlier observations, when a single particle was set in motion on a fixed rough bed (Ancey *et al.* 2003). Moreover, the order of magnitude of \bar{u}_r predicted by our theory is approximately 20 cm/s for $\tan \theta = 0.1$, while experimentally, \bar{u}_f was closer to 6 cm/s.

The same observation applies to the saltating particles, whose mean velocity exhibits little correlation with the mean fluid velocity. Contrary to the rolling velocity, the semi-empirical relation (2.23) intersects the data, but the dependence of the saltating velocity \bar{u}_s on \bar{u}_f is much more pronounced theoretically than experimentally.

Although the flows were dilute, there was no clear relation between the mean velocity of one particle of a system of N moving particles and the mean velocity of an isolated particle, which was entrained alone by a turbulent water stream. For the rolling regime, this may be quite easily understood: because the rolling particles moved on a mobile bed, the path was less regular in our bed-load experiments than in our earlier experiments, where a single particle was in motion down a corrugated stationary bottom. This probably induced an increase in the energy dissipation. What is difficult to understand, however, is the very weak dependence of \bar{u}_s on \bar{u}_f . This has important consequences in the computation of the solid discharge \dot{n} . Recall that $\dot{n} = \sum_{i=1}^N u_i v_p / L$, with v_p the particle volume; if the particle velocity $u_i \approx \bar{u}_p$ is nearly independent of \bar{u}_f , then we can approximate

$$\dot{n} \approx \frac{N v_p}{L} \bar{u}_p,$$

and the dependence of \dot{n} on \bar{u}_f is entirely contained in N . This contradicts the common assumption in Bagnold-like models, where the mismatch between the mean fluid and particle velocities is the control parameter of momentum transfers and thus of the solid discharge. This may explain why Bagnold's approach performs poorly at low water discharges.

4.6. Energy dissipation

In absence of particles, energy supplied by gravity is entirely dissipated by turbulent structures. When particles can be entrained, another energy sink is due to momentum and energy transfer between water and particles. To evaluate the efficiency of this energy sink, we compute the ratio of the turbulent power

$$P_t = \rho g q_w L \sin \theta - \bar{N} \bar{F}_D \bar{u}_p,$$

to the power supplied by gravity to the control volume

$$P_g = \int_{\mathcal{V}} \rho \mathbf{g} \cdot \mathbf{u} d\mathcal{V} = \rho g q_w L \sin \theta.$$

In the particle energy budget, we neglect the energy dissipated due to particle spin or lift force. The mean drag force was evaluated using the relation $\bar{F}_D = C_d \pi a^2 (\bar{u}_p - \bar{u}_f)^2 / 2$, with $C_d = 0.5$ the drag coefficient. In the numerical computations, we distinguished the particles in rolling and saltating regimes (see Tables 1 and 2).

Figure 17 shows how P_t/P_g varied with the bottom shear stress $\rho g h \sin \theta$. For gentle slopes ($\tan \theta < 0.1$) and moderate solid discharges ($\dot{n} < 16$ beads/s), almost all energy

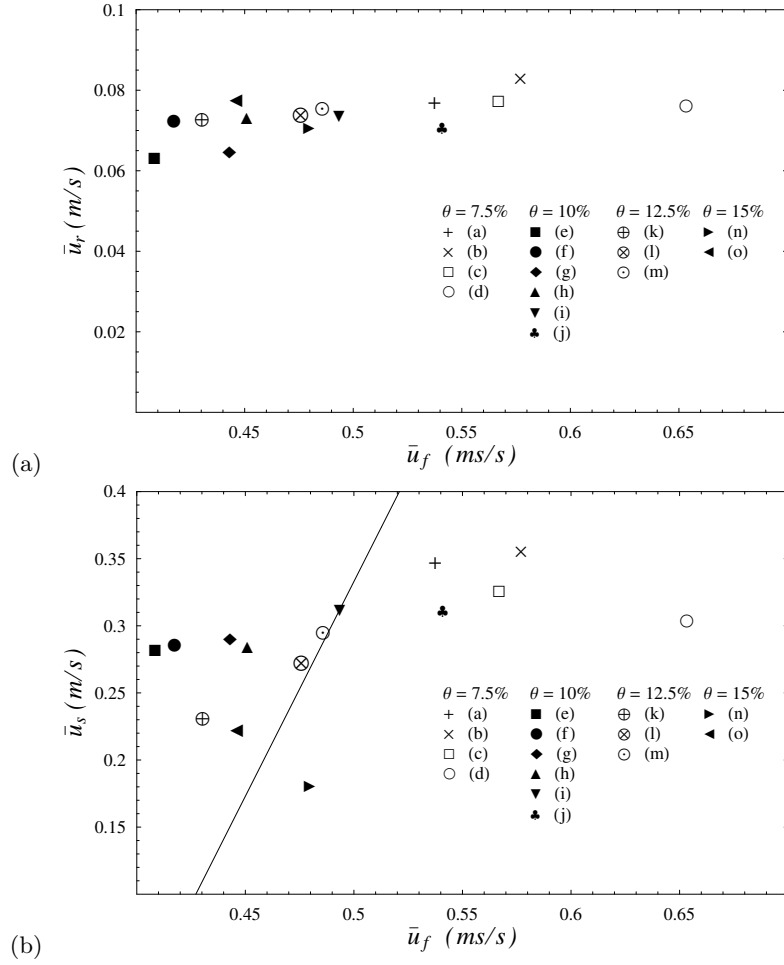
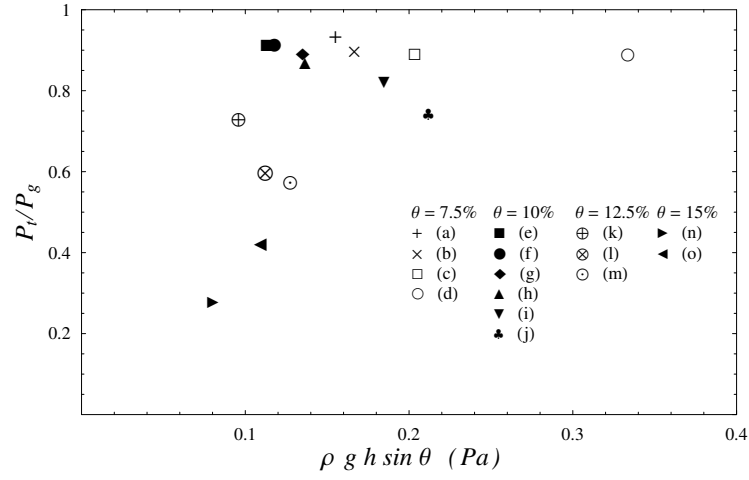


FIGURE 16. (a) Variation of the rolling velocity with the mean fluid velocity. (b) Variation of the saltating velocity with the mean fluid velocity; the solid line represents the velocity of a single isolated particle, as predicted by equation (2.23) for $\tan \theta = 0.1$.

was dissipated by turbulence—the ratio P_t/P_g remains close to 90%—independently of the bottom shear stress. When the solid discharge is increased or for steep slopes, there is a significant drop of the turbulent-energy contribution to the total energy. For instance, for run (o) ($\tan \theta = 0.15$ and $\dot{n} = 16$ beads/s), 25% of the energy supplied by gravity is dissipated by turbulence against 75% by momentum transfers with particles. As for particle velocity, the independence of the ratio P_t/P_g and \bar{u}_f indicated that for our experiments, there was no real coupling between the solid and water phases through energy balance, contrary to what is assumed in Bagnold's approach.

FIGURE 17. Variation in the ratio P_t/P_g with the bottom shear stress.

5. Concluding remarks

On the macroscopic scale, sediment transport seems physically simple since the solid discharge is usually found to be a linear function of the water discharge. If the problem is addressed from a mechanical perspective, the reasons why we observe this simple behaviour are still unclear despite much research over the last century. Recently, more fundamental experiments have been conducted to gain insight into the behaviour of particles and the connection between behaviour on the macroscopic and particle scales. Typical examples include the experimental and numerical investigations led by Schmeeckle & Nelson (2003), who tried to clarify the role of turbulence in incipient motion of coarse particles, or the experiments performed by Charru *et al.* (2004), who analysed entrainment and motion of coarse particles under laminar flow conditions. With the same objective in mind, we ran experiments in a narrow channel, where coarse particles (glass beads) were entrained by a turbulent water stream down a steep slope (7.5% to 15%). The particle trajectories being two-dimensional, we were able to measure numerous quantities, from the particle velocity to the number of entrainments/depositions per unit time. Although very idealized with respect to sediment transport in gravel-bed rivers, our experimental facility provides a realistic experimental basis for understanding the physical processes involved in sediment transport.

To interpret our data, we needed a theoretical framework. The intermittent nature of solid discharge at low water discharges led us to develop a stochastic model. This approach has its roots in Einstein's pioneering work (Einstein 1950), but although this earlier theory includes some ingredients essential to model sediment transport, it relies on statistical assumptions that have turned out to be unrealistic, thus undermining the entire approach. For instance, in Einstein's theory and subsequent variants, fluctuations of the solid discharge are Gaussian, whereas field and laboratory measurements show wider and more frequent fluctuations. In this paper, we proposed a simple theoretical model which essentially describes what happens within a control volume. The number of particles within this window can vary as a result of inflow, outflow, entrainment, and deposition of particles. Our model scrupulously follows this mass balance principle and adds a fundamental ingredient: particles arrive and leave the window randomly, and are entrained and deposited randomly. Mass balance results in a birth-death immigration-emigration Markov model. Two crucial assumptions are that particles can be entrained because of (i) water effects and (ii) collisions with moving particles. The latter assumption enables feedback between the moving particles and those at rest, which turns out to be essential for explaining the existence of wide fluctuations. Indeed, if we remove this feedback ($\mu = 0$), our model provides predictions that closely resemble Einstein's results.

A puzzling point is that in this purely counting vision of bed-load transport, we do not make the feedback dependent on water flow. Intuitively, we could expect that the water stream cannot entrain any number of particles, notably because of the energy constraint that limits particle entrainment and transportation. This would plead in favour of a control of water flow conditions on sediment transport via momentum transfers, as argued by Bagnold (1966, 1973) and subsequent authors (e.g., see Seminara *et al.* 2002). Within this approach, if some part P_p of the total energy supplied by gravity acceleration is allocated to particles' motion, then the total number of moving particles must satisfy

$$\bar{N} = P_p / (\bar{F}_D \bar{u}_p),$$

as shown in § 4.6. Here, it clearly appears experimentally that for bed inclinations as steep as 10%, flow was sufficiently dilute and vigorous for turbulence to be the main energy sink (see Figure 17); the energy dissipated by particle motion (P_p) does not exceed 15–20% of

the total and is independent of the fluid velocity. This contradicts Bagnold-like models: if P_p remains nearly constant, the number of moving particles should decrease with increasing fluid velocities if \bar{N} is controlled by momentum transfers. With our model, we have shown that the number of moving particles does not depend explicitly on the water flow conditions: to some extent (for $\mu > 0$), water flow dictates how many particles can be dislodged from the bed and entrained into the flow, but it loosely controls the number of settling particles and the number of particles set in motion because of collisions. In a steady state, the entrainment rate $E = \mu\bar{N} + \lambda_1(\bar{u}_f)$ must balance the deposition rate $D = \sigma\bar{N}$, which yields a variation in the total number of moving with fluid velocity in the form of a linear function (if μ and σ are constant)

$$\bar{N} = \frac{\lambda_1(\bar{u}_f)}{\sigma - \mu}.$$

With the solid discharge defined as the product of the number of moving particles N and the particle velocity, our theoretical model was then completed by computing the mean particle velocity. Surprisingly, this computation was not indispensable: for our experiments the mean velocity of a particular system did not depend strongly on fluid velocity (see figure 16), whereas for a single particle entrained by the turbulent stream, the particle velocity varies nearly linearly with the mean fluid velocity (Ancey *et al.* 2002, 2003). A striking and unanticipated result is that the linearity between solid discharge and fluid velocity stems mainly from the dependence of N on \bar{u}_f .

Our final stochastic model counts the number of moving particles, as depicted by Figure 2. The inflow rate is denoted by λ_0 , the outflow rate by ν , the deposition rate by σ ; for entrainment, we distinguish the entrainment rate induced by water (λ_1) from the collective entrainment rate (μ). For flows at equilibrium, the solid discharge \dot{n} corresponds to the inflow and outflow rates: $\dot{n} = \lambda_0 = \bar{N}\nu$. The other parameters depend on the size of the window and specifically on its length L , and the fluid velocity. We cannot compute these parameters analytically, but their dependence on \bar{u}_f can be anticipated. Experimentally, we found that μ and σ were almost constant [see Figure 15(c) and Table 3], whereas λ_1 was nearly proportional to the fluid velocity [see Figure 15(b)]. In the model, we did not discriminate between rolling and saltating particles; a natural development would be to distinguish these two species and to include additional equations to describe the population exchanges between them, which should enhance the model accuracy.

This stochastic model enables us to predict a number of salient statistical features characterizing the macroscopic behaviour of our system. The fluctuations in the solid discharge or the number of moving particles are well described (see Figure 9). The model also provides reasonably good estimates of the autocorrelation function and the statistical properties of deposition events for low solid discharges and gentle slopes. At higher solid discharges and for steep slopes, there is an increasing divergence between model predictions and our data, presumably reflecting the change in behaviour due to the increase in slope; this change was expected for slopes in excess of 10% (see § 2.5). We firmly believe that taking a closer look at statistical properties of solid discharge is of fundamental importance to understanding natural phenomena. Surprisingly, simple power-law models relating the sediment flow rate to the water flow depth can perform better than more sophisticated physically-based models (i.e., models that take into account a number of physical processes such as a threshold for incipient motion, nonlinear interaction with water velocity, etc.) for natural gravel-bed rivers (Barry *et al.* 2004). One possible explanation lies in the measurement protocols used in the field and laboratory. For gravel-bed rivers, hydraulicians and geomorphologists use various systems (Helley-Smith sampler,

bed-load trap) to measure bed load by capturing sediment over a given time interval. In the laboratory, hydraulicians impose the solid discharge at the flume inlet (hopper supplying the flume) or measure it at the outlet. For the former protocol, the crux of the issue lies in the proper selection of the sampling time (ranging from a few seconds to several minutes); this difficulty of selecting a proper time scale is illustrated by the large differences among various measurement systems (Bunte & Abt 2005). In § 2.6, we have found that the number of settling particles is negative binomial, with mean $r(1 - p')/p'$ [see equation (2.25)], where p' is a parameter that depends nonlinearly on the time interval δt during which the measurement is taken. From this perspective, this is little hope of establishing a direct link between trapped sediment and solid discharge without taking the random nature of transport into account. Experiments in the laboratory pose other problems: since bed load is imposed or measured at the inlet or outlet, one only has an idea of the number of particles that emigrate or immigrate (parameters ν and λ_0 of the model) from/into the control volume. At low water discharges, the mean waiting time between two entrainment events is long; if the typical duration of the experiment is shorter than the waiting time, it is likely that no emigrating particle is detected and one may conclude that the solid discharge is zero. From this perspective, the threshold for incipient motion is probably time-dependent at low water discharges, a point that is never taken into account in hydraulic computations and may explain the discrepancy between laboratory and field measurements.

Our model is sufficiently simple to provide analytical solutions in both steady and time-dependent conditions. Notably, once the model's entrainment coefficients λ_1 , μ , and σ are known (e.g., by estimating their values from data obtained with flows at equilibrium), we are able to describe the time evolution of the system [see equation (2.11)] when the flow is far from equilibrium. Physically, this makes sense because there is no strong coupling between the solid and water phases, as discussed earlier. Again, our description differs profoundly from earlier models, in which the control of sediment transport by water is a key assumption.

Experiments also suggest that the stochastic framework is well suited to intermediate solid discharges. The deviations between theoretical predictions and data are more and more significant with increasing slope and flow rate (i.e., Shields numbers). A current limitation of our experimental facility is that we cannot perform experiments over times of more than one minute, which forced us to select slopes and water flow rates with a sufficient number of events per experiment. It would be interesting to pursue the experimental investigation and comparison with the model at very low flow rates when a few particles are moving and can be entrained by the stream. This would test the model in more severe flow conditions.

REFERENCES

- ABBOTT, J. & FRANCIS, J. 1977 Saltation and suspension trajectories of solid grains in a water stream. *Proc. R. Soc. London* **284**, 225–254.
- ANCEY, C., BIGILLON, F., FREY, P. & DUCRET, R. 2003 Rolling motion of a single bead in a rapid shallow water stream down a steep channel. *Phys. Rev. E* **67**, 011303.
- ANCEY, C., BIGILLON, F., FREY, P., LANIER, J. & DUCRET, R. 2002 Motion of a single bead in a rapid shallow water stream down an inclined steep channel. *Phys. Rev. E* **66**, 036306.
- ANCEY, C., BÖHM, T., JODEAU, M. & FREY, P. 2006 Statistical description of sediment transport experiments. *Phys. Rev. E* **74**, 011302.
- ANCEY, C., EVESQUE, P. & COUSSOT, P. 1996 Motion of a single bead on a bead row: theoretical investigations. *J. Phys. I* **6**, 725–751.
- ARMANINI, A. & GREGORETTI, C. 2005 Incipient sediment motion at high slopes in uniform flow condition. *Water Resour. Res.* **41**, W12431.
- BAGNOLD, R. 1966 An approach to the sediment transport problem from general physics. Professional paper 422-i. Geological Survey.
- BAGNOLD, R. 1973 The nature of saltation and of ‘bed load’ transport in water. *Proc. R. Soc. London ser. A* **332**, 473–504.
- BAGNOLD, R. 1986 Transport of solids by natural water flow: evidence for a worldwide correlation. *Proc. R. Soc. London ser. A* **405**, 369–374.
- BALMFORTH, N. & PROVENZALE, A. 2001 Patterns of dirt. In *Geomorphological Fluid Mechanics* (ed. N. Balmforth & A. Provenzale), pp. 369–393. Berlin: Springer Verlag.
- BARRY, J., BUFFINGTON, J. & KING, J. 2004 A general power equation for predicting bed load transport rates in gravel bed rivers. *Water Resour. Res.* **40**, W10401.
- BÖHM, T., ANCEY, C., FREY, P., REBOUD, J.-L. & DUCOTTET, C. 2004 Fluctuations of the solid discharge of gravity-driven particle flows in a turbulent stream. *Phys. Rev. E* **69**, 061307.
- BÖHM, T., FREY, P., DUCOTTET, C., ANCEY, C., JODEAU, M. & REBOUD, J.-L. 2006 Two-dimensional motion of a set of particles in a free surface flow with image processing. *Exper. Fluids* **41**, 1–11.
- BRIDGE, J. & DOMINIC, D. 1984 Bed load grain velocities and sediment transport rates. *Water Resour. Res.* **20**, 476–490.
- BUNTE, K. & ABT, S. 2005 Effect of sampling time on measured gravel bed load transport rates in a coarse-bedded stream. *Water Resour. Res.* **41**, W11405.
- CHARRU, F., MOUILLERON, H. & EIFF, O. 2004 Erosion and deposition of particles on a bed sheared by a viscous flow. *J. Fluid Mech.* **519**, 55–80.
- CHENG, N.-S. 2004 Analysis of bedload transport in laminar flows. *Adv. Water Resour.* **27**, 937–942.
- CHENG, N.-S., TANG, H. & ZHU, L. 2004 Evaluation of bed load transport subject to high shear stress fluctuations. *Water Resour. Res.* **40**, W05601.
- COLES, S. 2001 *An Introduction to Statistical Modeling of Extreme Values*. London: Springer.
- COX, D. & MILLER, H. 1965 *The Theory of Stochastic Processes*. Boca Raton: Chapman & Hall CRC.
- DAVISON, A. 2003 *Statistical Models*. Cambridge: Cambridge University Press.
- DRAKE, T., SHREVE, R., DIETRICH, W. & LEOPOLD, L. 1988 Bedload transport of fine gravel observed by motion-picture photography. *J. Fluid Mech.* **192**, 193–217.
- EINSTEIN, H. 1950 The bed-load function for sediment transportation in open channel flows. *Tech. Rep.* Technical Report No. 1026. United States Department of Agriculture.
- ETTEMA, R. & MUTEL, C. 2004 Hans Albert Einstein: Innovation and compromise in formulating sediment transport by rivers. *J. Hydraul. Eng.* **130**, 477–487.
- FERNANDEZ LUQUE, R. & VAN BEEK, R. 1976 Erosion and transport of bed-load sediment. *J. Hydraul. Res.* **14**, 127–144.
- FREY, P., DUFRESNE, M., BÖHM, T., JODEAU, M. & ANCEY, C. 2006 Experimental study of bed load on steep slopes. In *River Flow 2006* (ed. R. M. L. Ferreira, E. Alves, J. G. A. B. Leal & A. Cardoso), vol. 1, pp. 887–893. Lisbon: Taylor & Francis.
- GARABEDIAN, P. 1964 *Partial Differential Equations*. New York: John Wiley & Sons.
- GARDINER, C. 1983 *Handbook of Stochastic Methods*. Berlin: Springer Verlag.

- GOMEZ, B. & CHURCH, M. 1989 An assessment of bed load sediment transport formulae for gravel bed rivers. *Water Resour. Res.* **25**, 1161–1186.
- GORDON, R., CARMICHAEL, J. & ISACKSON, F. 1972 Saltation of plastic balls in a one-dimensional flume. *Water Resour. Res.* **8**, 444–459.
- GRAF, W. 1984 *Hydraulics of Sediment Transport*. Littleton: Water Resources Publications.
- GRANT, G. 1997 Critical flow constrains flow hydraulics in mobile-bed streams: a new hypothesis. *Water Resour. Res.* **33**, 349–358.
- GRASS, A. 1970 Initial instability of fine bed sand. *J. Hydraul. Eng.* **96**, 619–632.
- IVERSON, R. 2003 How should mathematical models of geomorphic processes be judged? In *Prediction in Geomorphology* (ed. P. Wilcock & R. Iverson), pp. 83–94. Washington, D.C.: American Geophysical Union.
- JENKINS, J. & HANES, H. 1998 Collisional sheet flows of sediment driven by a turbulent fluid. *J. Fluid Mech.* **370**, 29–52.
- JULIEN, P.-Y. 1994 *Erosion and Sedimentation*. Cambridge: Cambridge University Press.
- KIRCHNER, J., DIETRICH, W., ISEYA, F. & IKEDA, H. 1990 The variability of critical shear stress, friction angle, and grain protrusion in water-worked sediments. *Sedimentology* **37**, 647–672.
- KLEINHANS, M. & VAN RIJN, L. 2002 Stochastic prediction of sediment transport in sand-gravel bed rivers. *J. Hydraul. Eng.* **128**, 412–425.
- KUHNLE, R. A. & SOUTHARD, J. B. 1988 Bed load transport fluctuations in a gravel bed laboratory channel. *Water Resour. Res.* **24**, 247–260.
- LAURSEN, E. 1958 The total sediment load of streams. *J. Hydraul. Div. ASCE* **84**, 1530.
- LAURSEN, E. 1999 Discussion on ‘Pickup probability for sediment entrainment’. *J. Hydraul. Eng.* **124**, 786–787.
- LISLE, I., ROSE, C., HOGARTH, W., HAIRSIEN, P., SANDER, G. & PARLANGE, J. Y. 1998 Stochastic sediment transport in soil erosion. *J. Hydrol.* **204**, 217–230.
- LISLE, T. 1989 Sediment transport and resulting deposition in spawning gravels, north coastal California. *Water Resour. Res.* **25**, 1303–1319.
- LOPEZ, F. & GARCÍA, M. 2001 Risk of sediment erosion and suspension in turbulent flows. *J. Hydraul. Eng.* **127**, 231–235.
- MARTIN, Y. 2003 Evaluation of bed load transport formulae using field evidence from the Vedder River, British Columbia. *Geomorphology* **53**, 75–95.
- NELSON, J., SCHMEECKLE, M. & SHREVE, R. 2001 Turbulence and particle entrainment. In *Gravel Bed Rivers* (ed. M. Mosley), pp. 221–248. Littleton: Water Resources Publications.
- NELSON, J., SHREVE, R., MCLEAN, S. & DRAKE, T. 1995 Role of near-bed turbulence structure in bed load transport and bed form mechanics. *Water Resour. Res.* **31**, 2071–2086.
- NEZU, I. & NAKAGAWA, H. 1993 *Turbulence in Open-Channel Flows*. Balkema.
- NIÑO, Y. & GARCÍA, M. 1994 Gravel saltation 2. Modeling. *Water Resour. Res.* **30**, 1915–1924.
- NIÑO, Y. & GARCÍA, M. 1998 Using Lagrangian particle saltation observations for bedload sediment transport modelling. *Hydrolog. Process.* **12**, 1197–1218.
- NIÑO, Y., GARCÍA, M. & AYALA, L. 1994 Gravel saltation 1. Experiments. *Water Resour. Res.* **30**, 1907–1914.
- NIKORA, V., HABERSACK, H., HUBER, T. & MCEWAN, I. 2002 On bed particle diffusion in gravel bed flows under weak bed load transport. *Water Resour. Res.* **38**, 10.1029/2001WR000513.
- NIKORA, V., HEALD, J., GORING, D. & MCEWAN, I. 2001 Diffusion of saltating particles in unidirectional water flow over a rough granular bed. *J. Phys. A: Math. Gen.* **34**, L743–L749.
- PAINTAL, A. 1971 A stochastic model of bed load transport. *J. Hydraul. Res.* **9**, 527–554.
- PAPANICOLAOU, A., DIPLAS, P., EVAGGELOPOULOS, N. & FOTOPOULOS, S. 2002 Stochastic incipient motion criterion for spheres under various bed packing conditions. *J. Hydraul. Eng.* **128**, 369–390.
- RAUDKIVI, A. 1990 *Loose Boundary Hydraulics*. Oxford: Pergamon Press.
- RICKENMANN, D. 2001 Comparison of bed load transport in torrents and gravel bed streams. *Water Resour. Res.* **37**, 3295–3306.
- VAN RIJN, L. 1985 Sediment transport, part I: bed load transport. *J. Hydraul. Eng.* **110**, 1431–1456.

- SCHMEECKLE, M. & NELSON, J. 2003 Direct numerical simulation of bedload transport using a local, dynamic boundary condition. *Sedimentology* **50**, 279–301.
- SEMINARA, G., SOLARI, L. & PARKER, G. 2002 Bed load at low Shield stress on arbitrariness sloping beds: failure of the Bagnold hypothesis. *Water Resour. Res.* **38**, 1249.
- SORNETTE, D. 2000 *Critical Phenomena in Natural Sciences*. New York: Springer.
- SUMER, B., CHUA, L., CHENG, N. & FREDSE 2003 Influence of Turbulence on Bed Load Sediment Transport. *J. Hydraul. Eng.* **129**, 585–596.
- WIBERG, P. & SMITH, J. 1985 A theoretical model for saltating grains in water. *J. Geophys. Res. C* **90**, 7341–7354.
- WIBERG, P. & SMITH, J. 1989 Model for calculating bedload transport of sediment. *J. Hydraul. Eng.* **115**, 101–123.
- WILCOCK, P. 2001 Toward a practical method for estimating sediment-transport rates in gravel bed-rivers. *Earth Surf. Processes Landforms* **26**, 1395–1408.
- YALIN, M. 1963 An expression for bed-load transportation. *J. Hydraul. Div. ASCE* **89**, 221–249.